Available online at www.sciencedirect.com
ScienceDirect
Journal of Computational Physics 225 (2007) 1442–1471
JOURNAL OF COMPUTATIONAL PHYSICS
www.elsevier.com/locate/jcp

Stretching-based diagnostics and reduction of chemical kinetic models with diffusion

A. Adrover [a,*], F. Creta [b], M. Giona [a], M. Valorani [b]

[a] *Dipartimento di Ingegneria Chimica, Facoltà di Ingegneria, Università di Roma "La Sapienza", via Eudossiana 18, 00184 Roma, Italy*
[b] *Dipartimento di Meccanica e Aeronautica, Facoltà di Ingegneria, Università di Roma "La Sapienza", via Eudossiana 18, 00184 Roma, Italy*

Received 22 July 2006; received in revised form 14 December 2006; accepted 31 January 2007
Available online 9 February 2007

Abstract

A new method for diagnostics and reduction of dynamical systems and chemical kinetic models is proposed. The method makes use of the local structure of the normal stretching rates by projecting the dynamics onto the local directions of maximal stretching. The approach is computationally very simple as it implies the spectral analysis of a symmetric matrix. Notwithstanding its simplicity, stretching-based analysis derives from a geometric basis grounded on the pointwise applications of concepts of normal hyperbolicity theory. As a byproduct, a simple reduction method is derived, equivalent to a "local embedding algorithm", which is based on the local projection of the dynamics onto the "most unstable and/or slow modes" compared to the time scale dictated by the local tangential dynamics. This method provides excellent results in the analysis and reduction of dynamical systems displaying relaxation towards an equilibrium point, limit cycles and chaotic attractors. Several numerical examples deriving from typical models of reaction/diffusion kinetics exhibiting complex dynamics are thoroughly addressed. The application to typical combustion models is also analyzed.

MSC: 65Lxx; 80A30; 64P05; 58xx

Keywords: Dynamical systems; Chemical kinetics; Model reduction; Slow manifolds; Invariant Geometric Properties; Normal hyperbolicity

1. Introduction

Many chemical, biochemical and biological processes involve a large number of species and reactions [1,2], and the resulting kinetic schemes, either under perfectly mixed condition or, a fortiori when spatial inhomogeneities (diffusion and/or convection) are accounted for, are expressed by means of high-dimensional dynamical systems. The occurrence of a large number of different time scales, and the resulting stiffness of the model equations are common features of all these models.

* Corresponding author. Tel.: +39 06 44585339; fax: +39 06 44585451.
E-mail address: alex@giona.ing.uniroma1.it (A. Adrover).

0021-9991/$ - see front matter
doi:10.1016/j.jcp.2007.01.030

In order to highlight the role and the influence of the different kinetic steps (model diagnostics), simplify the model equations, and possibly obtain a reduced model, different theoretical and computational approaches have been proposed, such as the Intrinsic Low-Dimensional Manifold (ILDM) method [3–5], Computational Singular Perturbation (CSP) [6,7], the Method of Invariant Manifold (MIM) [8,9], the method by Fraser and Roussel [10,11], methods based on Lyapunov functions such as the thermodynamic free energy [12,13], methods based on the intrinsic dynamics in the tangent/cotangent bundle [14], the Zero Time Derivative method [15], a combination of the Fraser and Roussel method with CSP [16]. For a review and a comparison of several of these approaches see [17,18].

The common denominator of all these computational strategies is a simple and evocative paradigm: the occurrence within the phase space of a Slow Invariant Manifold (SIM) for system dynamics, attracting nearby orbits, possessing a lower dimensionality than the phase space, and representing the backbone around which orbit dynamics is organized.

In the case of infinite-dimensional systems, such as reaction–diffusion models [19] expressed by means of a system of partial differential equations, the transposition of ILDM and CSP approaches have been proposed by Hadjinicolau and Goussis [20], Singh et al. [21], Goussis et al. [22], via the concept of an infinite-dimensional slow manifold obtained by projecting the dynamics onto the local slow modes associated with the kinetics. These approaches have been developed aside from the inertial manifold theory, proposed by Temam et al. [23,24] that provides functional–theoretical criteria and computational methods [25–28] to obtain a finite-dimensional representation of reaction–diffusion dynamics within an absorbing invariant set.

Motivated by the case study of singularly perturbed systems [29–31], considered as a benchmarking prototype, the recent literature on model simplification and reduction has been characterized by a superposition of tools and methods deriving from geometric concepts (essentially expressing manifold invariance), perturbation theory and computational strategies. CSP by Lam and Goussis [6,7], and the approach proposed in [16,32] provide examples of the superposition of paradigms.

Although the connection between singularly perturbed system and computational methods for model reduction in generic models is strong and motivated, it is important to observe that the formulation of reduction strategies for generic dynamical systems of physical interest is in general divorced from a perturbative analysis, and that singularly perturbed systems represent solely a nonexhaustive class of dynamical models which can be tackled and simplified by means of model reduction methods.

The intermingling of concepts deriving from singular perturbation theory, differential geometry and numerical analysis has provided a wealth of different computational strategies to tackle model simplification of complex kinetics schemes. On the other hand, some controversial issues have been raised on the definition of slow manifolds and their properties. The reason for this may be attributed to different reasons: (i) the conditions imposed by different authors on slow manifolds may have different nature (e.g. by imposing some smoothness and analyticity criteria on the local representation of the manifold itself that by other authors are neglected [33–35]); (ii) any geometrical definition of the slow manifold should be grounded on global properties defined throughout the entire phase space, including the behavior at infinity [36], while this may not be the case in perturbation studies; (iii) in practical applications to model reduction of complex kinetic schemes, ''intrinsic low-dimensional manifolds'' may lack some basic properties (such as invariance [37], see e.g. [38]), and this limitation ''collides'' with more formal mathematical definitions of slow invariant manifolds [39]. Correspondingly, the very basic concept of ''slow/fast decomposition'' of complex reaction schemes may involve some intrinsic degree of arbitrariness since it relies on the specific method adopted in model diagnostics and reduction (such as ILDM [3], CSP [7], MIM [8]).

Apart from these fundamental issues on the definition of slow invariant manifolds, it is important to observe that most of the computational strategies proposed for model simplification and reduction have been developed and tested for chemically reacting systems evolving towards a stable equilibrium point. The ILDM and CSP methods have been verified and benchmarked by considering chemical reacting systems and combustion models relaxing towards equilibria as paradigmatic examples [4,40]. It is, therefore, not surprising that the application of these model reduction techniques display problems and shortcomings when applied to dynamical systems evolving towards more general limit sets such as limit cycles and chaotic attractors [14]. In point of fact, the occurrence of persistent asymptotic oscillations defined on periodic/aperiodic/chaotic limit sets is a common feature observed in many chemical and biochemical open systems (closed adiabatic chemical systems

obeying the law of mass action, possess a unique stable equilibrium point). For a review, see the monographs by Scott and Goldbeter [41,42], and references cited therein.

As far as reduction strategies are concerned, the occurrence of more complex limit attractors introduces an extra degree of complexity to be taken into account. An efficient reduction algorithm for these dynamical systems should not only correctly describe the relaxation towards the limit set, but also the oscillating behavior on the invariant limit set itself. Several geometrical approaches have been proposed for tackling this wider class of dynamical systems, which are based on invariant vector dynamics within the tangent bundles [14,43,44]. All these approaches are theoretically extremely interesting, since they address invariant geometric features of dynamical systems on a fundamental level, but suffer the problem of being computationally onerous for higher-dimensional dynamical systems, as they require the explicit estimate of vector dynamics along system orbits. In the case one is interested in the reconstruction of the dynamics exclusively on invariant limit sets, a wealth of different approaches have been provided. For a review, see e.g. [45] and references cited therein.

The aim of this article is to propose a simple and efficient model reduction and diagnostic method for generic dynamical systems regardless of their finite or infinite-dimensional nature, and of the geometry of their limit sets. At the core of the method is a geometric characterization based on local normal stretching rates. The numerics requires the spectral characterization of a symmetric matrix.

In spite of its conceptual simplicity, the stretching-based method for system diagnostics is based on a geometric description of local tangent and normal dynamics. This geometric description finds its theoretical justification in the theory of normal hyperbolicity [39,46], viewed on a local level, i.e., pointwisely along system orbits. To some extent, the stretching-based method shares some analogies with some recent modification of ILDM [8,47]. However, there are some conceptual differences between the method proposed and these ILDM-based strategies, as discussed in the remainder of the article (Section 3).

The stretching-based reduction method can be viewed as a local embedding technique stemming from the stretching rate analysis of the system, obtained by locally projecting the dynamics onto the most unstable/slow directions. The reduction method proposed is computationally simple and efficient as it exclusively involves the solution of a lower-dimensional system of ordinary differential equations without nonlinear constraints, the dimension of which coincides with the number of relevant normal directions that should be locally accounted for.

The article is organized as follows. Section 2 reviews succinctly the basic notions of normal hyperbolicity and the definition of local normal/tangential stretching rates. Several examples taken from prototypical kinetic models highlight the meaning of the stretching-based analysis in the characterization of dynamic properties along system orbits and invariant manifolds. Section 3 introduces the stretching-based approach to model characterization in the general n-dimensional case and explores connections and differences with other existing methods. In particular, we show how to compute the normal stretching rate spectrum (and the corresponding set of directions of maximum normal stretching restricted to the normal subspace) and how it can be used for performing a local classification of the slow and fast (or unstable/stable) modes of the dynamics. Section 4 addresses the stretching-based method via some paradigmatic examples, by considering both low-dimensional models and nonlinear reaction–diffusion kinetics originating periodic and chaotic oscillations. The role of conservation laws in chemical kinetics is addressed in an Appendix, by considering the Michaelis–Menten enzymatic reaction as a prototypical model. Section 5 develops the stretching-based reduction method, and discusses several empirical criteria for defining the number of relevant normal modes. Apart from low-dimensional prototypical systems exhibiting chaotic behavior, the examples of application of the stretching-based reduction strategy concern infinite-dimensional reaction–diffusion systems and premixed flames.

2. Normal hyperbolicity and stretching rates

The theory of invariant manifolds of dynamical systems is grounded on the concept of *normal hyperbolicity* [39]. Essentially, given a map (diffeomorphism) ϕ of a manifold $\mathscr{M}$ onto itself, $\phi : \mathscr{M} \to \mathscr{M}$, a smooth submanifold $\mathscr{V}$, invariant under ϕ (i.e. such that $\phi(\mathscr{V}) \subseteq \mathscr{V}$) is normally hyperbolic if the tangent bundle $T\mathscr{M}|_{\mathscr{V}}$ of $\mathscr{M}$ restricted to $\mathscr{V}$ can be decomposed into three continuous sub-bundles:

$$T\mathscr{M}|_{\mathscr{V}} = \mathscr{N}^u \oplus T\mathscr{V} \oplus \mathscr{N}^s \tag{1}$$

where $T\mathscr{V}$ is the tangent bundle of $\mathscr{V}$, and $\mathscr{N}^u \oplus \mathscr{N}^s$ corresponds to a splitting of the normal bundle to $\mathscr{V}$ into an unstable and a stable sub-bundle. The two normal sub-bundles $\mathscr{N}^u$ and $\mathscr{N}^s$ are such that the vector dynamics generated by ϕ, i.e. the linear map $\mathrm{D}\phi : T\mathscr{M} \to T\mathscr{M}$ of the tangent bundle onto itself defined by the differential[1] $\mathrm{D}\phi$ of ϕ is such that:

(1) $\mathrm{D}\phi$ expands vectors of $\mathscr{N}^u$ more sharply than vectors of $T\mathscr{V}$,
(2) $\mathrm{D}\phi$ contracts vectors of $\mathscr{N}^s$ more sharply than vectors of $T\mathscr{V}$.

This definition of normal hyperbolicity is of global nature, i.e. it refers to the evolution of vectors in the sub-bundles $\mathscr{N}^u$, $\mathscr{T}\mathscr{V}$, $\mathscr{N}^s$. A local definition of normal hyperbolicity based on local rates of expansion and contraction, specifically suited for local diagnostics and model reduction, is given in the remainder of the article (see Eq. (26) and related discussion).

In general terms, therefore, the concept of normal hyperbolicity of a manifold indicates that the strength of the flow along the manifold is weaker than the attraction/repulsion to/from it [46]. Under the condition of normal hyperbolicity, a wealth of results can be established on the existence and persistence of invariant manifolds of dynamical systems, such as the Hadamard–Perron theorem regarding the existence of stable and unstable manifolds [39], and the Fenichel's results related to the persistence of invariant manifolds under perturbations [31]. The latter theorem is invoked in the singular perturbation theory of dynamical systems to confer a firm mathematical setting to perturbation methods and computational approaches aimed at decoupling slow and fast components of the dynamics, and at obtaining numerical approximations of slow invariant manifolds [37].

By focusing on dynamical systems possessing linearly stable (i.e. exponentially attracting [48]) slow invariant manifolds $\mathscr{W}$, the splitting of the tangent bundle expressed by Eq. (1) at any point $\mathbf{x} \in \mathscr{W}$ simplifies, since the unstable sub-bundle $\mathscr{N}^u$ is absent and $T\mathscr{M}|_{\mathscr{W}}$ can be decomposed as follows:

$$T\mathscr{M}|_{\mathscr{W}} = T\mathscr{W} \oplus \mathscr{N}^s \tag{2}$$

where vectors belonging to $\mathscr{N}^s$ are contracted by the action of the differential $\mathrm{D}\phi$ more sharply than vectors belonging to the tangent sub-bundle $T\mathscr{W}$ of $\mathscr{W}$. In the case of exponentially attracting manifolds, the requirement associated with the notion of normal hyperbolicity dictates that whatever the dynamics within the invariant manifold $\mathscr{W}$ is, normal vectors to $\mathscr{W}$ experience a more intense contraction (measured by their norms) than tangent vectors belonging to $T\mathscr{W}$. The latter property is also the most intuitive dynamic requirement for an exponentially attracting invariant manifold in order to be regarded as a "slow manifold".

The fact that an invariant exponentially attracting manifold should possess some form of normal hyperbolicity in order to be regarded as a "slow manifold" (in the intuitive and physically motivated meaning of this wording) is further addressed in this Section. A clear example of the importance of this property stems from the analysis of linear systems $\mathrm{d}\mathbf{x}/\mathrm{d}t = \mathbf{A}\mathbf{x}$, where $\mathbf{x} \in \mathbb{R}^n$, and the constant coefficient matrix $\mathbf{A}$ possesses distinct real and negative eigenvalues. For this class of systems, given any point $\mathbf{x}_0 \in \mathbb{R}^n$, the global orbit $O(\mathbf{x}_0)$ emanating from $\mathbf{x}_0$, i.e. the union of forward and backward orbits originating from $\mathbf{x}_0$, is an invariant and exponentially attracting one-dimensional manifold. However, solely the linear eigenmanifold passing through the origin $\mathbf{0}$ and spanned by the slowest eigenvector possesses the property that normal perturbations to it decay faster than tangential perturbations, thus motivating the claim that this manifold is the slow invariant one-dimensional manifold of the system[2].

The concept of normal hyperbolicity can be formulated in a way convenient to develop methods for model reduction alternative to the existing ones, and explicitly accounting for the dynamic properties of normal/tangential vectors. To this purpose, it is convenient to introduce the concept of tangential and normal stretching rates, in order to reformulate the analysis on a local basis.

First, let us consider the case of two-dimensional dynamical systems (the extension to higher-dimensional dynamics is developed in the next section).

[1] By choosing a coordinate system of $\mathscr{M}$, $\mathbf{x} = (x_1, \ldots, x_n)$, and letting $\mathbf{v} \in T\mathscr{M}_{\mathbf{x}}$, the action of the differential $\mathrm{D}\phi$ onto $\mathbf{v}$, is represented by the linear system $\mathrm{D}\phi\mathbf{v} = \mathbf{A}\mathbf{v}$, where $\mathbf{A} = \partial\phi(\mathbf{x})/\partial\mathbf{x}$ is the Jacobian matrix of ϕ.

[2] Analogously, the m-dimensional eigenmanifold, passing through the origin and spanned by the first m smallest eigenvalues, is actually a slow invariant manifold such that normal perturbations to it decay faster than tangential ones.

Let

$$\frac{\mathrm{d}\mathbf{x}}{\mathrm{d}t} = \mathbf{f}(\mathbf{x}) \tag{3}$$

be a two-dimensional dynamical system defined in $\mathbb{R}^2$, and let us further suppose that the system possesses a one-dimensional invariant slow-manifold $\mathscr{W}$ associated with the unique stable equilibrium point $\mathbf{x}^* = \mathbf{0}$, so that $\mathbf{f}(\mathbf{x}^*) = \mathbf{f}(\mathbf{0}) = \mathbf{0}$. Vector dynamics in the tangent bundle is described by the equation

$$\frac{\mathrm{d}\mathbf{v}}{\mathrm{d}t} = \mathbf{J}(\mathbf{x})\mathbf{v} \tag{4}$$

where $\mathbf{J}(\mathbf{x}) = \partial\mathbf{f}(\mathbf{x})/\partial\mathbf{x}$ is the Jacobian matrix of the vector field $\mathbf{f}(\mathbf{x})$ and $\mathbf{v}$ is a vector of the tangent bundle. By taking the scalar product of the left- and right-hand side of Eq. (4) with $\mathbf{v}$, it follows that

$$\frac{\mathrm{d}|\mathbf{v}|^2}{\mathrm{d}t} = 2(\mathbf{J}\mathbf{v},\mathbf{v}) = \frac{2(\mathbf{J}\mathbf{v},\mathbf{v})}{|\mathbf{v}|^2}|\mathbf{v}|^2 \tag{5}$$

where $|\mathbf{v}|$ indicates the norm of $\mathbf{v}$, and $(\mathbf{v},\mathbf{w})$ the scalar product between the two vectors $\mathbf{v}$ and $\mathbf{w}$. Eq. (5) implies that the stretching rate experienced by the generic vector $\mathbf{v}$ at point $\mathbf{x}$ is given by

$$\omega(\mathbf{x},\mathbf{v}) = \frac{(\mathbf{J}(\mathbf{x})\mathbf{v},\mathbf{v})}{|\mathbf{v}|^2} = (\mathbf{J}(\mathbf{x})\hat{\mathbf{v}},\hat{\mathbf{v}}) \tag{6}$$

or equivalently as $\omega(\mathbf{x},\mathbf{v}) = (\mathbf{J}^s(\mathbf{x})\hat{\mathbf{v}},\hat{\mathbf{v}})$, where $\hat{\mathbf{v}} = \mathbf{v}/|\mathbf{v}|$ is the unit vector associated with $\mathbf{v}$, $\mathbf{J}^s(\mathbf{x}) = (\mathbf{J}(\mathbf{x}) + \mathbf{J}^{\mathrm{T}}(\mathbf{x}))/2$ is the symmetric part of $\mathbf{J}(\mathbf{x})$, where $\mathbf{J}^{\mathrm{T}}$ is the transpose of $\mathbf{J}$.

Let us now consider the dynamics of tangent and normal vectors to the invariant manifold[3] $\mathscr{W}$, which in the present case is one-dimensional. The tangential and normal stretching rates $\omega_\tau(\mathbf{x})$ and $\omega_\nu(\mathbf{x})$ at any point $\mathbf{x} \in \mathscr{W}$ are given by

$$\omega_\tau(\mathbf{x}) = (\mathbf{J}(\mathbf{x})\hat{\mathbf{f}},\hat{\mathbf{f}}) \tag{7}$$

$$\omega_\nu(\mathbf{x}) = (\mathbf{J}(\mathbf{x})\hat{\mathbf{n}},\hat{\mathbf{n}}) \tag{8}$$

where $\hat{\mathbf{f}} = \mathbf{f}/|\mathbf{f}|, \hat{\mathbf{n}} = \mathbf{n}/|\mathbf{n}|$, and $\mathbf{n} = (f_2, -f_1), f_1$ and f_2 being the two entries of the vector field $\mathbf{f}$. Note that Eq. (7) stems from the fact that $\mathscr{W}$ is invariant for the dynamical system Eq. (3), and correspondingly the tangent space at $\mathbf{x} \in \mathscr{W}$ is spanned by the vector field $\mathbf{f}(\mathbf{x})$ itself.

The tangential and normal stretching rates provide a local (pointwise) way to characterize stretching dynamics and, as a byproduct, the dynamics within invariant manifolds. Let $\boldsymbol{\tau}_{\mathbf{x}_0}(t)$ and $\boldsymbol{\nu}_{\mathbf{x}_0}(t)$ be the vectors evolved at time t starting from $\boldsymbol{\tau}(0) \in T\mathscr{W}_{\mathbf{x}_0}$ and $\boldsymbol{\nu}(0) \in N\mathscr{W}_{\mathbf{x}_0}$, respectively, and let $\Pi^{\nu}_{\mathbf{x}}$ be the normal projector at a point $\mathbf{x}$, which maps any vector into its orthogonal component to $T\mathscr{W}_{\mathbf{x}}$. It follows from Eq. (5) after some algebra[4] that

[3] Henceforth, given an invariant manifold $\mathscr{W}$, the normal sub-bundle, i.e. the orthogonal complement to its tangent sub-bundle $T\mathscr{W}$, is indicated with the symbol $N\mathscr{W}$. Therefore, $T\mathscr{W}_{\mathbf{x}}$ and $N\mathscr{W}_{\mathbf{x}}$ are the tangent and the normal subspaces at the point $\mathbf{x} \in \mathscr{W}$, respectively.

[4] Eq. (10) describing the dynamics of normal components can be simply derived as follows. Consider the dynamics of a generic vector $\mathbf{v}$, starting from a generic initial vector $\mathbf{v}_0$ possessing nonvanishing components both in the central (spanned by $\mathbf{f}$) and in the normal subspaces. For any time $t > 0$, let $\mathbf{v}(t) = \phi_t^*(\mathbf{z})\mathbf{v}_0$, where ϕ_t is the phase flow and $\phi_t^*(\mathbf{z}) = \partial\phi_t(\mathbf{z})/\partial\mathbf{z}$. The vector $\mathbf{v}(t)$ can be expressed as $\mathbf{v} = a\mathbf{f} + \mathbf{n}$, where $\mathbf{f} = \mathbf{f}(\phi_t(\mathbf{z}))$ is the vector field, a is a scalar depending on time and $\mathbf{n}(t) = \Pi^{\nu}_{\phi_t(\mathbf{z})}[\mathbf{v}(t)]$, is the normal component of $\mathbf{v}$. By definition, both $\mathbf{v}$ and $\mathbf{f}$ satisfy the equation for vector dynamics $\mathrm{d}\mathbf{v}/\mathrm{d}t = \mathbf{J}\mathbf{v}$ and $\mathrm{d}\mathbf{f}/\mathrm{d}t = \mathbf{J}\mathbf{f}$. By differentiating the expression for $\mathbf{v}$ with respect to time and substituting into it the expressions for the time derivatives of $\mathbf{v}$ and $\mathbf{f}$, it follows that $\mathrm{d}\mathbf{n}/\mathrm{d}t = \mathbf{J}\mathbf{n} - \mathbf{f}\mathrm{d}a/\mathrm{d}t$. The latter equation implies that the normal sub-bundle is not invariant because of the presence of the the extra term $\mathbf{f}\mathrm{d}a/\mathrm{d}t$ that appears aligned in the tangential direction. In order to get rid of this term, one can take the scalar product with respect to $\mathbf{n}$, so that $(\mathrm{d}\mathbf{n}/\mathrm{d}t, \mathbf{n}) = (\mathbf{J}\mathbf{n}, \mathbf{n}) - \mathrm{d}a/\mathrm{d}t(\mathbf{f}, \mathbf{n})$. By considering that, by definition, $(\mathbf{f}, \mathbf{n}) = 0$, the latter expression implies that

$$\frac{\mathrm{d}|\mathbf{n}|^2}{\mathrm{d}t} = 2(\mathbf{J}\hat{\mathbf{n}},\hat{\mathbf{n}})|\mathbf{n}|^2 \;\Rightarrow\; |\mathbf{n}(t)| = |\mathbf{n}(0)|\exp\left(\int_0^t \omega_\nu(\mathbf{z}(t'))\mathrm{d}t'\right)$$

where $\omega_\nu = (\mathbf{J}\hat{\mathbf{n}},\hat{\mathbf{n}})$ and $\hat{\mathbf{n}} = \mathbf{n}/|\mathbf{n}|$. A similar procedure can be followed for deriving Eq. (9).

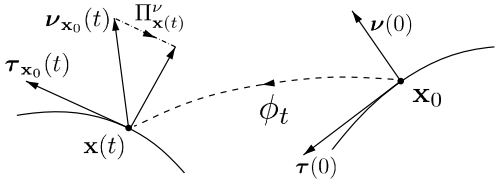

Fig. 1. Schematic evolution of normal and tangential vectors along an invariant one-dimensional manifold $\mathscr{W}$. ϕ_t is the phase flow, $\mathbf{x}(t) = \phi_t(\mathbf{x}_0)$ associated with Eq. (3).

$$|\boldsymbol{\tau}_{\mathbf{x}_0}(t)| = |\boldsymbol{\tau}(0)| \exp\left[\int_0^t \omega_\tau(\mathbf{x}(t'))\mathrm{d}t'\right] \tag{9}$$

$$|\Pi^{v}_{\mathbf{x}(t)}[\boldsymbol{v}_{\mathbf{x}_0}(t)]| = |\boldsymbol{v}(0)| \exp\left[\int_0^t \omega_v(\mathbf{x}(t'))\mathrm{d}t'\right] \tag{10}$$

where $\mathbf{x}(t)$ is the solution of the Cauchy problem associated with Eq. (3) and with the initial condition $\mathbf{x}(t=0) = \mathbf{x}_0$. The geometrical meaning of Eqs. (9), (10) is depicted in Fig. 1. Observe that the normal projector $\Pi^{v}_{\mathbf{x}(t)}$ is used in Eq. (10). This is essential because the normal sub-bundle is not invariant and, therefore, the evolution of any normal vector introduces a component belonging to the tangent sub-bundle.

Tangential and normal stretching rates, estimated along an invariant manifold $\mathscr{W}$, provide a pointwise characterization of the dynamics of tangential and normal perturbations to the manifold $\mathscr{W}$. From this observation it follows that a local characterization of normal hyperbolicity and the identification of the slow and fast (and more generally of the unstable and stable) components of the dynamics on an invariant manifold can be obtained by considering the behavior of normal and tangential stretching rates and their relative strength.

It is convenient to exemplify this observation via a numerical example. Consider the Semenov model for thermal explosions [49,50], which represents the evolution of a first-order exothermic reaction in a perfectly stirred batch system in the presence of heat exchange with the surrounding. In dimensionless form, the heat and mass balance equations read [38]

$$\varepsilon\frac{\mathrm{d}x}{\mathrm{d}t} = (yq(x) - x\delta), \quad \frac{\mathrm{d}y}{\mathrm{d}t} = -yq(x) \tag{11}$$

where x and y are the dimensionless temperature and reactant concentration, respectively, and $q(x) = \exp(x/(1+\beta x))$. The parameter β is the reciprocal of the Zeldovich number, i.e. of the dimensionless activation energy, normalized with respect to the coolant temperature. We fix[5] $\delta = 1, \beta = 0.31$, and let the parameter ε vary. This system has been thoroughly analyzed elsewhere [36] in terms of the structure of the invariant slow manifolds, the bifurcations occurring by changing the parameter values and the way these bifurcations affect slow manifold properties. For $\varepsilon < 1$, the system possesses a unique global slow manifold[6] $\mathscr{W}_s$. Figs. 2(a) and (b) (bold lines) show the portion of the global slow manifold near the point $\mathbf{x}^*$ for two values of $\varepsilon = 10^{-3}, 10^{-2}$.

Since the relative strength of normal to tangent perturbations is significant to qualify the properties of a slow manifold, the stretching ratio $r(\mathbf{x})$:

$$r(\mathbf{x}) = \frac{\omega_v(\mathbf{x})}{\omega_\tau(\mathbf{x})}, \quad \mathbf{x} \in \mathscr{W}_s \tag{12}$$

provides a lumped local indicator of the normal-to-tangential stretching.[7]

[5] The choice of the values for the parameter δ and β is indeed immaterial in the present analysis. Any other choice for these parameter values would produce qualitatively similar results.

[6] The global slow manifold is the heteroclinic connection between the equilibrium point $\mathbf{x}^* = \mathbf{0} = (0,0)$ and a saddle point at infinity [51]. The saddle-point at infinity can be easily obtained by compactifying the system, i.e. by considering the Poincaré projection of Eq. (11) on the sphere-at-infinity [52].

[7] At almost all the points $\mathbf{x}$ the stretching ratio is a bounded function of the position. However, there are points at which $r(\mathbf{x})$ diverges. The numerator $\omega_v(\mathbf{x})$ cannot diverge to infinity if the Jacobian is bounded. However, the denominator $\omega_\tau(\mathbf{x})$ can be equal to zero at any point at which the time derivative of the modulus of the vector field along the trajectory passing through it vanishes. This means that the acceleration $\mathrm{d}\mathbf{f}/\mathrm{d}t$ is orthogonal to the velocity $\mathbf{f}$.

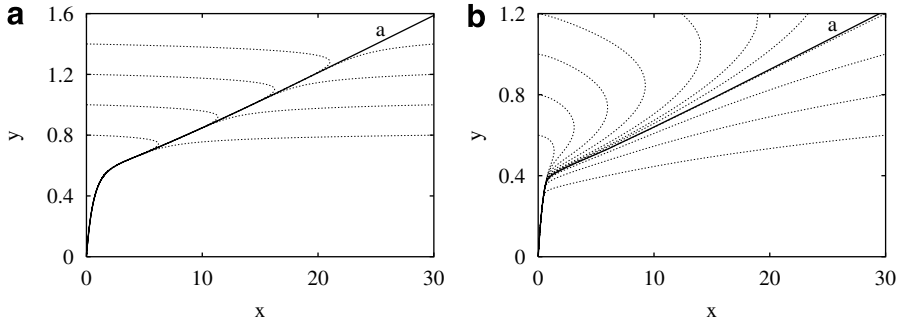

Fig. 2. Phase portrait of the Semenov explosion model for $\beta = 0.31$: (a) $\varepsilon = 10^{-3}$, (b) $\varepsilon = 10^{-2}$. Marked line (a) indicates the global slow manifold of the equilibrium $\mathbf{x}^*$.

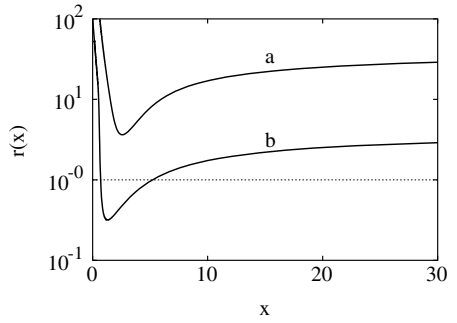

Fig. 3. Stretching ratio $r(x)$ vs x along the global slow manifold of the Semenov model $\beta = 0.31$: (a) $\varepsilon = 10^{-3}$, (b) $\varepsilon = 10^{-2}$.

The behavior of $r(x)$ as a function of the x-coordinate along the global slow manifold $\mathcal{W}_s$ is depicted in Fig. 3.

For $\varepsilon = 10^{-3}$ (curve a in Fig. 3), the stretching ratio is strictly and uniformly greater than 1. This indicates that, throughout the whole manifold $\mathcal{W}_s$, normal vectors are contracted more sharply than tangential ones. This phenomenon corresponds to a locally normally hyperbolic slow manifold, i.e. of a "well-behaved" slow invariant manifold attracting nearby orbits, as can be observed from the phase-space plot depicted in Fig. 2(a). On the contrary, for $\varepsilon = 10^{-2}$ (Fig. 3, curve b) there exists a portion of the slow manifold (referred to as the *inverting zone*), in the range $x \in (0.52, 5.22)$, for which $r(x) < 1$. In this interval, the contraction of normal perturbations is weaker than the tangential dynamics, and this affects orbit dynamics, as illustrated in the phase-space plot depicted in Fig. 2(b): system orbits travel close but almost parallel to the slow manifold in the inverting region.

In the perspective of model reduction, the dynamics in the neighborhood of the inverting region can hardly be viewed as purely one-dimensional and "localized" on $\mathcal{W}_s$, because the evolution of normal perturbations is no longer faster than tangential evolution. Hence local normal hyperbolicity of $\mathcal{W}_s$, viewed as a one-dimensional and invariant manifold, is lost. This observation can be generalized to higher-dimensional systems, which are the subject of the remainder of this article. In all the cases in which a local inversion at a point $\mathbf{x}$ along a manifold $\mathcal{W}_s$ occurs in the behavior of normal-to-tangential stretching rates, a local slow manifold $\mathcal{W}_{\mathrm{loc}}(\mathbf{x})$ at $\mathbf{x}$ can be defined by augmenting the dimensionality of $\mathcal{W}_s$ in order to accommodate, within the now-augmented tangent bundle of $\mathcal{W}_{\mathrm{loc}}(\mathbf{x})$, the slower or more unstable directions. This operation can be viewed as a linear embedding of $\mathcal{W}_s$ into $\mathcal{W}_{\mathrm{loc}}(\mathbf{x})$ at $\mathbf{x}$.

This two-dimensional example indicates that it is possible, and indeed convenient, to develop a stretching-based approach aimed at: (i) quantifying, on a local basis, the properties of slow manifolds, (ii) identifying, from a stretching-based viewpoint, the slow and fast (unstable/stable) components of the dynamics, (iii) developing simple and computationally efficient methods for model analysis and reduction grounded on the relative strength of normal to tangential stretching rates.

3. The stretching-based approach

In order to develop a stretching-based description of slow and fast components of a dynamic evolution aimed at identifying approximate slow manifolds, it is necessary to generalize the concept of normal stretching rates and their estimate for dynamical systems defined on a n-dimensional phase-space with $n > 2$. The next subsection addresses this issue, and subsequently the stretching-based approach to model reduction is introduced.

3.1. The n-dimensional case

This Section generalizes the characterization of normal hyperbolicity for manifolds defined in n-dimensional phase spaces with $n > 2$. Let us first consider a one-dimensional manifold $\mathscr{W}$ (e.g. an orbit) of an n-dimensional dynamical system. While the tangential stretching rate can be estimated according to Eq. (7), the definition of normal stretching rates requires some more algebra and further additional observations. A way of defining $\omega_v(\mathbf{x})$ is the following:

$$\omega_v(\mathbf{x}) = \max_{\hat{\mathbf{n}} \in N\mathscr{W}_{\mathbf{x}} | \hat{\mathbf{n}}|=1} (\mathbf{J}(\mathbf{x})\hat{\mathbf{n}}, \hat{\mathbf{n}}) \tag{13}$$

where the maximum is taken over all the normal unit vectors belonging to the normal space $N\mathscr{W}_{\mathbf{x}}$ at $\mathbf{x}$.

The estimate of ω_v and the consequent introduction of a spectrum of normal stretching rates can be performed as follows. Let $\mathbf{x} \in \mathscr{W}$ and $\mathbf{f}(\mathbf{x})$ be the vector field at the point. The first step is to obtain a basis for $N\mathscr{W}_{\mathbf{x}}$. Let h be the index corresponding to the maximum entry of $\mathbf{f}(\mathbf{x}) = (f_1, \ldots, f_n)$ in absolute value:

$$h : |f_h(\mathbf{x})| = \max \;\Rightarrow\; |f_k(\mathbf{x})| \leqslant |f_h(\mathbf{x})|, \quad k \neq h \tag{14}$$

Let $\mathbf{e}_1 = (1, 0, \ldots, 0), \mathbf{e}_2 = (0, 1, \ldots, 0)$, etc. be the unit vectors oriented towards the coordinate axes of the phase space. If $h \neq 1$ choose

$$\mathbf{B} = \{\hat{\mathbf{f}}(\mathbf{x}), \mathbf{e}_1, \mathbf{e}_2, \ldots, \mathbf{e}_{h-1}, \mathbf{e}_{h+1}, \ldots, \mathbf{e}_n\} \tag{15}$$

otherwise take

$$\mathbf{B} = \{\hat{\mathbf{f}}(\mathbf{x}), \mathbf{e}_2, \mathbf{e}_3, \ldots, \mathbf{e}_{n-1}, \mathbf{e}_n\} \tag{16}$$

It is straightforward to see that the system of vectors defined by Eqs. (15) or (16) is by construction linearly independent, and consequently it forms a basis for the tangent space $T\mathbb{R}^n$ at $\mathbf{x}$. The vector basis $\mathbf{B}$ can be made orthonormal, by using e.g. the classical Gram–Schmidt procedure to obtain a new (orthonormal) basis $\widehat{\mathbf{B}} = \{\hat{\mathbf{e}}_h\}_{h=1}^n$, where $\hat{\mathbf{e}}_1 = \hat{\mathbf{f}}$. As a byproduct, the system of vectors $\hat{\mathbf{e}}_2, \ldots, \hat{\mathbf{e}}_n$ spans the normal subspace $N\mathscr{W}_{\mathbf{x}}$, and can be used as a orthonormal basis for the normal subspace.

By expressing the Jacobian matrix with respect to the new basis $\widehat{\mathbf{B}}$, the new matrix representation for $\mathbf{J}$ reads as

$$\widehat{\mathbf{J}} = \mathbf{T}^{-1}\mathbf{J}\mathbf{T} = \mathbf{T}^{\mathrm{T}}\mathbf{J}\mathbf{T} \tag{17}$$

where $\mathbf{T}$ is the matrix associated with the change of basis, i.e. such that $\widehat{\mathbf{B}} = \mathbf{I}\mathbf{T}$ where $\mathbf{I}$ is the identity matrix. Due to the orthonormality of $\widehat{\mathbf{B}}$, the matrix $\mathbf{T}$ is a unitary matrix, i.e. such that $\mathbf{T}^{\mathrm{T}} = \mathbf{T}^{-1}$, where $\mathbf{T}^{\mathrm{T}}$ is the transpose of $\mathbf{T}$. Componentwise, the matrix $\widehat{\mathbf{J}}$ reads

$$\widehat{\mathbf{J}} = \left(\begin{array}{c|ccccc} \hat{J}_{1,1} & \hat{J}_{1,2} & \hat{J}_{1,3} & \cdots & \cdots & \hat{J}_{1,n} \\ \hline \hat{J}_{2,1} & \hat{J}_{2,2} & \hat{J}_{1,3} & \cdots & \cdots & \hat{J}_{2,n} \\ \cdots & \cdots & \cdots & \cdots & \cdots & \cdots \\ \cdots & \cdots & \cdots & \cdots & \cdots & \cdots \\ \hat{J}_{n,1} & \hat{J}_{n,2} & \hat{J}_{n,3} & \cdots & \cdots & \hat{J}_{n,n} \end{array}\right) = \left(\begin{array}{c|c} \hat{\mathbf{J}}^{tt} & \hat{\mathbf{J}}^{tn} \\ \hline \hat{\mathbf{J}}^{nt} & \hat{\mathbf{J}}^{nn} \end{array}\right) \tag{18}$$

As a visual aid, the matrix $\widehat{\mathbf{J}}$ in Eq. (18) is partitioned into four blocks. By definition, since $\hat{\mathbf{e}}_1 = \hat{\mathbf{f}}$, any vector $\hat{\mathbf{n}} \in N\mathscr{W}_{\mathbf{x}}$ admits a vanishing first entry $\hat{n}_1 = 0$ so that the normal stretching rate associated with any $\hat{\mathbf{n}}$ is given by

$$\omega(\mathbf{x}, \hat{\mathbf{n}}) = \sum_{h=2}^{n} \sum_{k=2}^{n} \widehat{J}_{h,k} \hat{n}_h \hat{n}_k \tag{19}$$

and, therefore, solely the block $\widehat{\mathbf{J}}^{nn}$ in Eq. (18) matters in defining normal stretching rates. Consequently, the maximum normal stretching rate corresponds to the maximum of the quadratic form Eq. (19) subjected to the constraint

$$\sum_{h=2}^{n} \hat{n}_h^2 = 1 \tag{20}$$

This extremal problem, with the constraint expressed by Eq. (20), corresponds to the extremum of the quadratic objective function

$$\Omega(\hat{n}_2, \ldots, \hat{n}_n; \lambda) = \sum_{h=2}^{n} \sum_{k=2}^{n} \widehat{J}_{h,k} \hat{n}_h \hat{n}_k - \lambda \left(\sum_{h=2}^{n} \hat{n}_h^2 - 1 \right) \tag{21}$$

where λ is a Lagrange multiplier. This extremal problem leads to the system of equations

$$\frac{\partial \Omega}{\partial \hat{n}_h} = 0, \; h = 2, \ldots, n \;\; \Rightarrow \;\; \sum_{k=2}^{n} \left[\frac{\widehat{J}_{h,k} + \widehat{J}_{k,h}}{2} \right] \hat{n}_k = \lambda \hat{n}_h, \quad h = 2, \ldots, n \tag{22}$$

Therefore, the estimate of ω_v reduces ultimately to an eigenvalue/eigenvector problem for the $(n-1) \times (n-1)$ symmetric matrix $\widehat{\mathbf{J}}^s$, the entries of which are

$$\widehat{J}^s_{h-1,k-1} = \frac{\widehat{J}_{h,k} + \widehat{J}_{k,h}}{2}, \quad h, k = 2, \ldots, n \tag{23}$$

Since $\widehat{\mathbf{J}}^s$ is symmetric, it possesses real eigenvalues μ_h, that can be ordered in a nonincreasing way, i.e. $\mu_1 \geqslant \mu_2 \geqslant \cdots \geqslant \mu_{n-1}$. The associated unit eigenvectors $\boldsymbol{\sigma}_1, \ldots, \boldsymbol{\sigma}_{n-1}$ are mutually orthonormal (if the eigenvalues are distinct), and form a basis for $N\mathscr{W}_{\mathbf{x}}$. Moreover each eigenvector $\boldsymbol{\sigma}_h$ generates a one-dimensional subspace $N\mathscr{W}_{\mathbf{x},h} \subset N\mathscr{W}_{\mathbf{x}}$ so that the $(n-1)$-dimensional normal subspace can be generated as the direct sum of each, i.e. $N\mathscr{W}_{\mathbf{x}} = \oplus_{h=1}^{n-1} N\mathscr{W}_{\mathbf{x},h}$.

The spectrum of eigenvalues of $\widehat{\mathbf{J}}^s$ coincides with the *pointwise normal stretching rate spectrum*

$$\Sigma_v(\mathbf{x}) = \{\omega_{v,h}(\mathbf{x})\}_{h=1}^{n-1} = \{\mu_h\}_{h=1}^{n-1} \tag{24}$$

The value of $\omega_v(\mathbf{x})$ defined by Eq. (13), therefore, is the largest eigenvalue of $\widehat{\mathbf{J}}^s$,

$$\omega_v(\mathbf{x}) = \omega_{v,1}(\mathbf{x}) = \mu_1 \tag{25}$$

and the corresponding direction of maximum normal stretching is spanned by $\boldsymbol{\sigma}_1 \in N\mathscr{W}_{\mathbf{x},1}$. The second eigenvector $\boldsymbol{\sigma}_2 \in N\mathscr{W}_{\mathbf{x},2}$ is associated with the maximum normal stretching rate $\omega_{v,2}(\mathbf{x}) = \mu_2$ within $\oplus_{h=2}^{n-1} N\mathscr{W}_{\mathbf{x},h}$, i.e. within the orthogonal complement to $T\mathscr{W}_{\mathbf{x}} \oplus N\mathscr{W}_{\mathbf{x},1}$. Analogously, the generic normal stretching rate $\omega_{v,\ell}(\mathbf{x})$, with $\ell \leqslant n-1$, is the maximum over the normal subspace $\oplus_{h=\ell}^{n-1} N\mathscr{W}_{\mathbf{x},h}$.

It should be observed that recent ILDM-based approaches have introduced symmetrized versions of the Jacobian matrix in order to simplify the computation of approximate invariant manifolds [8,47]. Gorban and Karlin [8] suggest the use of the symmetrized Jacobian $\mathbf{J}^{\mathrm{sym}} = (\mathbf{J} + \mathbf{J}^{\mathrm{T}})/2$, and propose a Symmetrized Entropic ILDM (SEILDM), in which the local Jacobian matrix is substituted by the symmetrized form $\mathbf{J}_e^{\mathrm{sym}} = (\mathbf{J} + \mathbf{H}_{\mathrm{c}}^{-1}\mathbf{J}^{\mathrm{T}}\mathbf{H}_{\mathrm{c}})/2$, where $\mathbf{H}_{\mathrm{c}}$ is the Hessian matrix of a Lyapunov function near the equilibrium. This approach applies solely near a stable equilibrium point $\mathbf{x}_e$, $\mathbf{f}(\mathbf{x}_e) = 0$. Bykov et al. [47] propose the TILDM method, in which the ILDM-basis vectors are replaced by the eigenvectors[8] of the symmetric matrix $\mathbf{M} = \mathbf{J}^{\mathrm{T}}\mathbf{J}$.

[8] It should be observed that the eigenvalues of the symmetric matrix $\mathbf{M}$ are the singular values of $\mathbf{J}$; by construction, they are all real and positive, this latter property preventing us to extract any information about the local stability properties of the system.

There are, however, some important differences between Eq. (23) and these approaches. The main difference is that Eq. (23) derives from a geometric principle: consider the normal perturbations to the driving direction $\hat{\mathbf{f}}(\mathbf{x})$ at $\mathbf{x}$, and obtain in the normal subspace the directions of maximum normal stretching. Observe that these directions are not the directions of maximum stretching for $\mathbf{J}$ (which correspond to the eigenvectors of $(\mathbf{J}+\mathbf{J}^{\mathrm{T}})/2$), but the directions of maximum normal stretching restricted to the normal subspace. This is the reason why the symmetrization is not performed over the whole Jacobian matrix but solely on a portion of it, after a suitable change of basis. This geometric perspective is not present in the other symmetrization approaches, in which the focus is mainly algebraic (to get rid of complex conjugate eigenvalues/eigenvectors of the Jacobian), while it represents the core of the current analysis (see further Section 5 and the development of a stretching-based reduction strategy).

The extension to higher-dimensional manifolds is straightforward, and follows the same approach developed above. Let $\mathscr{W}$ be a m-dimensional ($m>1$) manifold, invariant for the dynamical system Eq. (3), embedded in an n-dimensional phase space. Let $\mathbf{t}_1(\mathbf{x}),\ldots,\mathbf{t}_m(\mathbf{x})$ be an orthonormal system of vectors spanning the tangent space of $T\mathscr{W}_{\mathbf{x}}$ at the point $\mathbf{x}\in\mathscr{W}$. This tangent basis can be completed with a system of $n-m$ orthonormal vectors $\mathbf{e}_1,\ldots,\mathbf{e}_{n-m}$ belonging to the orthogonal complement $N\mathscr{W}_{\mathbf{x}}$.

Therefore, $\mathbf{B}=\{\mathbf{t}_1(\mathbf{x}),\ldots,\mathbf{t}_n(\mathbf{x}),\mathbf{e}_1,\ldots,\mathbf{e}_{n-m}\}$ is an orthonormal basis for $T\mathbb{R}^n$. By projecting the dynamical system on this local basis, the transformed Jacobian matrix $\widehat{\mathbf{J}}$ can be partitioned into the four blocks $\widehat{\mathbf{J}}^{tt},\widehat{\mathbf{J}}^{tn},\widehat{\mathbf{J}}^{nt}$ and $\widehat{\mathbf{J}}^{nn}$ (see Eq. (18)) and the the normal stretching rates can be obtained by considering the quadratic form associated with the $(n-m)\times(n-m)$ matrix $\widehat{\mathbf{J}}^{nn}$.

The latter generalization allows us to define the concept of *local normal hyperbolicity* and how it relates to the theory of normal hyperbolicity introduced at the beginning of Section 2. The concept of normal hyperbolicity can be formulated at a local level, by introducing the following definition. An m-dimensional manifold $\mathscr{W}$, invariant and exponentially attracting for the n-dimensional dynamical system Eq. (3) (with $n>m$) is locally normally hyperbolic at $\mathbf{x}\in\mathscr{W}$, if there is a $\tau>0$ such that the linear map $\mathrm{D}\phi_\tau$ associated with the phase flow ϕ_t for $t=\tau$ generated by the vector field $\mathbf{f}(\mathbf{x})$ contracts vectors of $\mathscr{N}^s$ more sharply than vectors of $T\mathscr{W}$. The time τ depends in general on $\mathbf{x}$. If this property holds for any $\mathbf{x}\in\mathscr{W}$, then the manifold $\mathscr{W}$ is uniformly locally normal hyperbolic. Since, this definition holds locally, it can be formulated in terms of stretching rates.

Specifically, let $\mathscr{W}$ be an m-dimensional manifold passing through $\mathbf{x}$, let $\omega_{\tau,1}(\mathbf{x}),\ldots,\omega_{\tau,m}(\mathbf{x})$ be the maximum tangential stretching rates experienced by vectors belonging to $T\mathscr{W}_{\mathbf{x}}$ and $\omega_{v,1}(\mathbf{x}),\ldots,\omega_{v,n-m}(\mathbf{x})$ the corresponding maximum normal stretching rates obtained as discussed above. Both $\omega_{\tau,1}(\mathbf{x}),\ldots,\omega_{\tau,m}(\mathbf{x})$, and $\omega_{v,1}(\mathbf{x}),\ldots,\omega_{v,n-m}(\mathbf{x})$ are ordered in a nonincreasing way. The general criterion of local normal hyperbolicity implies that

$$\omega_{\tau,m}(\mathbf{x})>\omega_{v,1}(\mathbf{x}) \tag{26}$$

i.e. that at least the smallest tangential rate is greater than the largest normal rate. If $\omega_{v,1}(\mathbf{x})<0$ this implies *locally*, i.e. in a neighborhood of $\mathbf{x}$, that normal perturbations decay faster than tangential ones.

On the other hand, the theory of normal hyperbolicity implies the splitting of the tangent space expressed by Eqs. (1) or (2), which is to be interpreted as a global, not local, decomposition. By considering the case of linearly stable manifolds, such that Eq. (2) applies, normal hyperbolicity implies a condition on the global evolution of normal and tangent vectors to $\mathscr{W}$. For any normal vector $\boldsymbol{v}(0)\in N\mathscr{W}_{\mathbf{x}_0}$, its evolution $\boldsymbol{v}_{\mathbf{x}_0}(t)$ at time t,

$$\boldsymbol{v}_{\mathbf{x}_0}(t)=\boldsymbol{v}_{\mathbf{x}_0,v}(t)+\boldsymbol{v}_{\mathbf{x}_0,\tau}(t) \tag{27}$$

where $\boldsymbol{v}_{\mathbf{x}_0,v}(t)\in N\mathscr{W}_{\mathbf{x}(t)},\boldsymbol{v}_{\mathbf{x}_0,\tau}(t)\in T\mathscr{W}_{\mathbf{x}(t)}$ is such that

$$|\boldsymbol{v}_{\mathbf{x}_0,v}(t)|=|\Pi_{\mathbf{x}(t)}[\boldsymbol{v}_{\mathbf{x}_0}(t)]|\leqslant C_v e^{-\lambda_v t}|\boldsymbol{v}(0)| \tag{28}$$

where $C_v,\lambda_v>0$. At the same time, the evolution of any tangent vector $\boldsymbol{\tau}(0)\in T\mathscr{W}_{\mathbf{x}_0}$ satisfies the inequality

$$|\boldsymbol{\tau}_{\mathbf{x}_0}(t)|\leqslant C_\tau \mathrm{e}^{\lambda_\tau t}|\boldsymbol{\tau}(0)| \tag{29}$$

where $C_\tau>0$, and λ_τ can be either positive or negative. In any case for generic normal and tangential vectors normal hyperbolicity implies that

$$\lambda_\tau>-\lambda_v \tag{30}$$

which essentially means that normal vectors contract more "sharply" than vectors belonging to the tangent sub-bundle to $\mathscr{W}$. We observe, however, that the constants C_v and C_τ entering Eqs. (28), (29) may attain values greater than 1. This could imply, solely on a local level, that normal vectors may grow, i.e. normal vector dynamics may be unstable (or slower than tangential dynamics), albeit linear stability and normal hyperbolicity of the manifold being guaranteed.

Clearly, local normal hyperbolicity implies a much weaker statement on the evolution of normal and tangential perturbations to $\mathscr{W}$, namely the fact that normal vectors locally experience stretching rates that are smaller than the stretching rates characterizing tangent vectors to $\mathscr{W}$.

3.2. Normal stretching spectrum and model reduction

The analysis of the normal stretching rates can be used for model diagnostics and reduction of complex systems. In order to address this issue, consider a dynamical system Eq. (3) defined in $\mathbb{R}^n$ and a generic point $\mathbf{x}$ of the phase space. At the point $\mathbf{x}$ one may consider the orbit passing through the point, and define the tangential stretching rate $\omega_\tau(\mathbf{x})$ and the normal stretching spectrum $\Sigma_v(\mathbf{x}) = \{\omega_{v,1}(\mathbf{x}), \ldots, \omega_{v,n-1}(\mathbf{x})\}$ ordered in a nondecreasing way and defined in Section 3.1. From the relative strength of the elements of $\Sigma_v(\mathbf{x})$ compared to the tangential rate $\omega_\tau(\mathbf{x})$, simple criteria for model decomposition can be inferred by exploiting the concept of local normal hyperbolicity.

Indeed, the tangential stretching rates yield the actual characteristic time scale $t_c(\mathbf{x}) = 1/\omega_\tau(\mathbf{x})$, the local driving time scale that should be compared with the time scales associated with the evolution of normal perturbations, represented by the normal spectrum $\Sigma_v(\mathbf{x})$.

Suppose that $\omega_\tau(\mathbf{x}) < 0$ and that $\omega_{v,1}(\mathbf{x}) < \omega_\tau(\mathbf{x})$. This implies that all the normal perturbations decay faster than the driving time-scale $t_c(\mathbf{x})$ associated with the vector field. Consequently, the orbit passing through the point $\mathbf{x}$ can be viewed locally (i.e. in a neighborhood of the point $\mathbf{x}$ itself) as a one-dimensional invariant normally hyperbolic manifold for the dynamical system Eq. (3).

On the contrary, let us suppose that the first $m > 0$ normal stretching rates are greater than ω_τ. This means that the normal perturbations in the directions spanned by the corresponding eigenvectors are either locally unstable (if the corresponding stretching rates are positive) or locally slower (for $\omega_{v,1} < 0$) than the characteristic time-scale associated with the decay of the intensity of the vector field, and expressed by the reciprocal of the tangential stretching rate. This implies that the one-dimensional invariant manifold passing through $\mathbf{x}$ ceases to be locally normally hyperbolic.

In the latter case, we can define in the neighborhood of $\mathbf{x}$ a $(m+1)$-dimensional embedding manifold $\mathscr{W}_{\mathrm{loc}}(\mathbf{x})$ which indeed is locally normally hyperbolic, by constructing its tangent space by means of the vector $\hat{\mathbf{f}}$, parallel to the vector field, and the vectors $\mathbf{s}_1, \ldots, \mathbf{s}_m$, where

$$\mathbf{s}_h = \mathbf{T}\boldsymbol{\sigma}_h, \quad h = 1, \ldots, m \tag{31}$$

are the eigenvectors associated with the first m directions of maximum normal stretching expressed in the canonical basis $\mathbf{e}_1, \ldots, \mathbf{e}_n$ and $\mathbf{T}$ is the matrix associated with the change of basis, Eq. (17).

In other words, the tangent subspace of $\mathscr{W}_{\mathrm{loc}}(\mathbf{x})$ is spanned by the vector field itself and by the vectors associated with those normal perturbations, the stretching rates of which are greater than $\omega_\tau(\mathbf{x})$.

The concept described above is the starting point for model diagnostics and reduction of complex dynamical systems, since it performs locally a classification of the slow and fast (unstable/stable) modes of the dynamics. The main issue in this classification is that the concept of slow and fast modes depends locally on the central time-scale t_c i.e. on the local rate of tangential evolution along the orbits. Slow/unstable modes correspond to normal perturbations along those directions possessing a normal stretching rate greater than ω_τ. Faster/more stable modes are those associated with normal rates smaller than ω_τ. Therefore, the tangential stretching acts as a threshold by setting the pace of what is locally slow or fast. A byproduct of this approach is the possibility of defining the dimension $N_{\mathrm{loc}}(\mathbf{x})$ of the local slow manifold $\mathscr{W}_{\mathrm{loc}}(\mathbf{x})$, from the condition

$$N_{\mathrm{loc}}(\mathbf{x}) = m + 1, \quad m : \omega_{v,m}(\mathbf{x}) \geqslant \omega_\tau(\mathbf{x}), \quad \omega_{v,m+1}(\mathbf{x}) < \omega_\tau(\mathbf{x}) \tag{32}$$

The criterion Eq. (32) for defining $N_{\mathrm{loc}}(\mathbf{x})$ should be commented further. Essentially, it means that the behavior of the system near $\mathbf{x}$ can be approximated by means of a $N_{\mathrm{loc}}(\mathbf{x})$-dimensional manifold $\mathscr{W}_{\mathrm{loc}}(\mathbf{x})$ which is

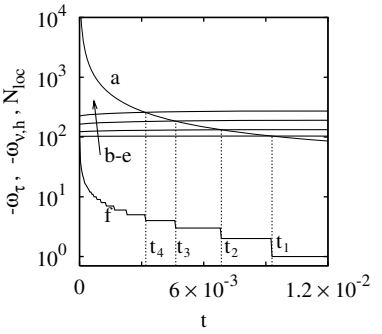

Fig. 4. $-\omega_\tau, -\omega_{v,h}$ and N_{loc} along a trajectory as a function of time for the reaction–diffusion system Eq. (33) for $\phi^2 = 10, K_m = 0.1n = 100$. Curve (a) depicts $-\omega_\tau$. Curves (b)–(e), indicated by the arrow, show the behavior of the first four $-\omega_{v,h}$, respectively. Curve (f) refers to the evolution of N_{loc}.

locally normally hyperbolic. Such local approximation is intrinsically not invariant, since normal vectors associated with the maximum normal stretching rates are not invariant for the vector dynamics expressed by Eq. (4). The lack of invariance is the *trade-off to be paid* in order to develop a simple computational method for model simplification and reduction. The criterion expressed by Eq. (32) proves to be a safe local criterion to ascertain that in the neighborhood of $\mathbf{x}$ normal perturbations are "overwhelming" in comparison to the dynamics of vectors tangent to $\mathscr{W}_{\mathrm{loc}}(\mathbf{x})$. Moreover, a complete characterization of the normal perturbations and of their influence on the dynamics can be achieved by examining the spectrum of normal stretching rates. Particularly interesting is the stretching rate analysis for chemical kinetics in the presence of conservation laws (induced by stoichiometric constraints). This case is thoroughly analyzed in Appendix A.

4. Numerical examples and stretching analysis

This Section addresses the stretching-based characterization of dynamical systems by considering several prototypical models to illustrate it.

4.1. Reaction–diffusion in a porous catalyst

In order to illustrate the stretching-based analysis, consider a classical reaction–diffusion equation

$$\partial_t c = \partial_x^2 c - \frac{\phi^2 c}{K_m + c}, \quad c|_{x=1} = 1, \quad \partial_x c|_{x=0} = 0 \tag{33}$$

where $\partial_x^m c = \partial^m c/\partial x^m$, defined on $x \in (0,1)$. This equation corresponds to the spatially one-dimensional approximation for a catalytic process within a porous solid catalyst, the reaction rate of which is expressed by a Langmuir–Hinshelwood kinetics. In Eq. (33), ϕ^2 is the square of the Thiele modulus, which is the ratio between the characteristic diffusion time to that of reaction. Let $c|_{t=0} = 0$, i.e. no reactant is initially present within the pore. Stretching-based analysis has been performed on a discretization of Eq. (33) by adopting a finite-difference scheme with $n = 100$ internal points.[9] Fig. 4 summarizes the result of the stretching analysis

[9] We adopted a three-points finite-difference approximation of the Laplacian and a forward finite-difference approximation of the first-order derivative entering the boundary condition at $x = 0$. The resulting set of n ODEs for the n time dependent variables $\{c_h\}_{h=1}^n$ is the following:

$$\mathrm{d}c_1/\mathrm{d}t = (c_2 - c_1)/\Delta x^2 - \phi^2 c_1/(K_m + c_1)$$
$$\mathrm{d}c_h/\mathrm{d}t = (c_{h+1} - 2c_h + c_{h-1})/\Delta x^2 - \phi^2 c_h/(K_m + c_h), \quad h = 2, \ldots, n$$

where $c_{n+1} = 1$ and $\Delta x = 1/(n+1)$. $n = 100$ internal points for the finite-difference discretization ensure a good resolution of the fundamental length scales of the systems, for all the time instants. The set of ODEs has been integrated by means a fourth-order Runge–Kutta algorithm.

for this system as it shows the behavior of $-\omega_\tau$ (curve a), $-\omega_{v,h}$ (curves b–e) and N_{loc} (line f) along a generic trajectory.

At short time scales, the initial reactant profile is discontinuous, since boundary and initial conditions do not match continuously at $x = 1$, hence the driving time scales, controlled by the action of the Laplacian operator, are very small. Almost all the normal modes are slower than t_c, and $N_{\mathrm{loc}} \simeq n$. As time increases, high frequency modes relax, and N_{loc} monotonically decreases up to $N_{\mathrm{loc}} = 1$ for large t. This phenomenon is clearly depicted in Fig. 4, where the staircase-like profile for N_{loc} (curve f) corresponds to the progressive extinguishment of all the remaining normal modes up to $t = t_1$, starting from which solely the dominant mode prevails ($N_{\mathrm{loc}} = 1$), and all the normal perturbations are extinguished. Each jump in the staircase-like profile for N_{loc} corresponds to the occurrence of the condition $-\omega_{v,h} > -\omega_\tau$ at the time instant t_h, $h = n-1,\ldots,1$, which corresponds to the monotone relaxation of the system dynamics onto lower-dimensional slow manifolds of dimension h. Only the last four time instants t_h, $h = 1,\ldots,4$ are shown in Fig. 4.

4.2. Low-dimensional chaotic dynamical systems

Stretching analysis applies to generic dynamical systems, including those exhibiting complex persistent oscillations such as chaotic models. To highlight this issue, consider the classical Lorenz system [53], which is the prototype for low-dimensional chaos in smooth time-continuous dynamics [54]

$$\begin{aligned}\dot{x} &= \sigma(y-x)\\ \dot{y} &= rx - y - xz\\ \dot{z} &= xy - bz\end{aligned} \tag{34}$$

where $\dot{x} = \mathrm{d}x/\mathrm{d}t$. Fig. 5(a) depicts the Lorenz attractor for $\sigma = 10, r = 28$ and $b = 8/3$, while Fig. 5(b) depicts the behavior of the tangential and normal stretching rates as a function of time t along a trajectory starting from a point on the Lorenz attractor. The Lorenz system has been integrated by means of a fourth-order Runge–Kutta algorithm. As expected, the stretching rates oscillate following the chaotic nature of the limit set. Specifically, it can be observed that for almost all the time instants the tangential stretching rate (depicted with a bold line) is greater than the second normal stretching rate $\omega_{v,2}$, and this implies $N_{\mathrm{loc}} = 2$ for almost all the times. We also observe that the number N^+ of positive stretching rates is always smaller than or equal to 2, since $\omega_{v,2} < 0$ uniformly. The numbers N_{loc} and N^+ will be used in the remainder of this article to develop criteria for model reduction of oscillating/chaotic dynamics (see Section 5).

Starting from the local definition of normal and tangential stretching rates, it is possible to introduce global quantities, obtained by averaging over time

$$\langle\omega_\tau\rangle(t) = \frac{1}{t}\int_0^t \omega_\tau(\phi_{t'}(\mathbf{x}_0))\mathrm{d}t', \quad \langle\omega_{v,h}\rangle(t) = \frac{1}{t}\int_0^t \omega_{v,h}(\phi_{t'}(\mathbf{x}_0))\mathrm{d}t', \;\; h = 1,\ldots,n-1 \tag{35}$$

The limit for $t \to \infty$ of these averages defines n real numbers that will be referred to as the pseudo-Lyapunov tangential/normal exponents

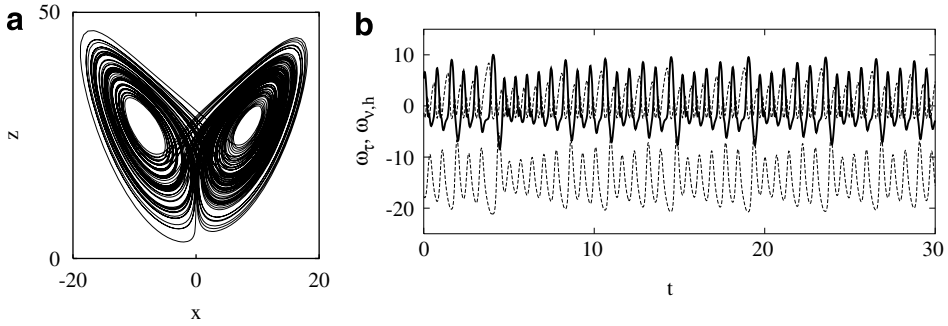

Fig. 5. (a) Projection of the Lorenz attractor for $\sigma = 10, r = 28$ and $b = 8/3$ onto the $x - z$ plane. (b) Evolution of the tangential (bold line) and normal (dashed lines) stretching rates vs t on the Lorenz attractor.

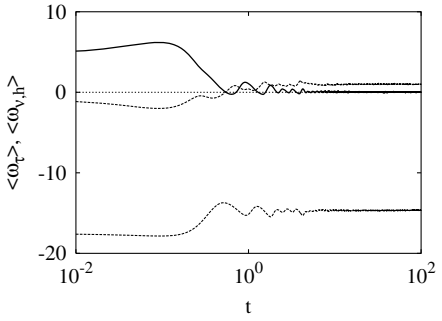

Fig. 6. Averaged tangential (bold line) and normal (dashed lines) stretching rates for the Lorenz system at $\sigma = 10, r = 28$ and $b = 8/3$.

$$\Lambda_\tau = \lim_{t\to\infty}\langle\omega_\tau\rangle(t), \quad \Lambda_{v,h} = \lim_{t\to\infty}\langle\omega_{v,h}\rangle(t) \tag{36}$$

Such *pseudo-Lyapunov spectrum* is not an invariant property of dynamical systems, since the normal directions of maximum stretching are not invariant. Therefore, it should not be confused with the Lyapunov spectrum that is defined by Oseledec's theorem [55] by means of the stretching/contracting behavior within invariant sub-bundles. More precisely, the spectrum of Lyapunov exponent emerges from the representation of the tangent bundle as the direct sum of invariant sub-bundles, and the Lyapunov exponents are the stretching exponents associated with the vector evolution within each of these invariant sub-bundles. The application of these concepts in model reduction is given in [14,56]. The stretching-based method makes no use of global invariant properties within the tangle bundle, but rather analyzes the local tangential and normal stretching rates pointwisely. This is the main difference of the SBR method, with respect to other methods such as NTDRB [14] or the method by Mease and Topcu [56], the core of which is the determination of the invariant sub-bundles (or filtrations), which represent the most suitable geometrical setting for expressing the timescale-properties of a dynamical system. Consequently, the definition of the pseudo-Lyapunov exponents is conceptually different from the spectrum of Lyapunov exponents. Solely qualitative connections between these two spectra can be derived, as discussed below (see Eqs. (37) and (38)).

Although the normal pseudo-Lyapunov quantities are not invariant exponents in the meaning of Oseledec's theorem, they may give useful information about global dynamics. Fig. 6 depicts the behavior of the averaged tangential and normal stretching rates for the Lorenz system.

The values for the pseudo-Lyapunov exponents[10] are: $\Lambda_\tau = 0, \Lambda_{v,1} = 0.986, \Lambda_{v,2} = -14.65$. These values should be compared with the true Lyapunov spectrum $\Lambda_{\mathrm{Lyap},h}$, $h = 1,2,3$, which in this case is given by $\Lambda_{\mathrm{Lyap},1} = 0.90 \pm 0.005, \Lambda_{\mathrm{Lyap},2} = 0, \Lambda_{\mathrm{Lyap},3} = -14.56 \pm 0.005$ [57]. The pseudo-Lyapunov exponents are sufficiently close to the correct Lyapunov spectrum. Moreover, it is important to observe that for any dynamical system

$$\Lambda_\tau + \sum_{h=1}^{n-1}\Lambda_{v,h} = \langle Tr(\mathbf{J})\rangle = \sum_{h=1}^{n}\Lambda_{\mathrm{Lyap},h} \tag{37}$$

where $\langle \mathrm{Tr}(\mathbf{J})\rangle$ is the time average of the trace of the Jacobian along a generic trajectory.[11]

In the case of the three-dimensional Lorenz model, Eq. (37) implies $\Lambda_{v,1} + \Lambda_{v,2} = \Lambda_{\mathrm{Lyap},1} + \Lambda_{\mathrm{Lyap},3} = -\sigma - b - 1$. A second property of the pseudo-Lyapunov spectrum is

$$\Lambda_{v,1} \geqslant \max_{h=1,\ldots,n}\Lambda_{\mathrm{Lyap},h} \tag{38}$$

[10] For dynamical systems possessing a periodic/aperiodic/chaotic attractor the tangential pseudo-Lyapunov number equals zero. This stems from the fact that the tangent sub-bundle for vector dynamics is spanned by the vector field itself which, being bounded in norm along the attractor, expresses neither a vector contraction nor elongation.

[11] Eq. (37) for the pseudo-Lyapunov exponents derives directly from the following property of the tangential and normal stretching rates $\omega_\tau + \sum_{h=1}^{n-1}\omega_{v,h} = \mathrm{Tr}(\mathbf{J})$. This property of the stretching rate spectrum can be simply derived by observing that $\mathrm{Tr}(\mathbf{J}) = \sum_{h=1}^{n}(\mathbf{J}\mathbf{w}_h, \mathbf{w}_h)$, where $\{\mathbf{w}_h\}_{h=1}^{n}$ is any orthonormal basis, and by applying it to the stretching-based orthonormal basis $\{\hat{\mathbf{e}}_h\}_{h=1}^{n}$.

i.e. the first normal pseudo-Lyapunov exponent is always greater than the maximum Lyapunov exponent of the system. The maximum Lyapunov exponent corresponds to the average stretching rate experienced along the most unstable invariant sub-bundle. At each point, this stretching rate is less than or at most equal to the local maximum normal stretching rate. This property is rather significant in terms of the stretching-based estimate of the embedding dimension of a dynamical system's global attractor (see Section 5). In particular, due to the lack of invariance of the normal sub-bundles, it is to be expected that the positive portion of the pseudo-Lyapunov spectrum is systematically larger than the corresponding portion of the Lyapunov spectrum. The number N_{pL}^{+} of positive pseudo-exponents will also be used in Section 5 to develop criteria for model reduction.

4.3. Chaotic reaction–diffusion models

As a typical reaction–diffusion model exhibiting a rich dynamic structure, we consider a model proposed by Elezgaray and Arneodo [58], henceforth referred to as the EA model for short. The EA model is a system of two coupled nonlinear partial differential equations in $u(x,t), v(x,t), x \in [0,1]$, representing the concentrations of two chemical species in a isothermal explosive kinetics displaying intermittent bursting for some values of the parameters

$$\begin{aligned} \partial_t u &= D\partial_x^2 u + \varepsilon^{-1}[v - (u^2 + u^3)] \\ \partial_t v &= D\partial_x^2 v - u + \alpha \end{aligned} \tag{39}$$

where D is the dimensionless diffusivity, and α, ε are positive parameters. The system Eq. (39) is equipped with boundary conditions on the concentration values

$$u(0,t) = u(1,t) = u_b = -2, \quad v(0,t) = v(1,t) = v_b = -4, \qquad t > 0 \tag{40}$$

This system of PDEs has been analyzed numerically by Elezgaray and Arneodo [58] by means of finite-differences, by Adrover et al. [59] by means of collocation methods, and by Graham and Kevrekidis [60] by means of spectral methods, by considering the bifurcation properties of the system with respect to the dimensionless diffusivity $D \in [0.02, 0.04]$ and keeping the other parameters fixed ($\alpha = 0.01, \varepsilon = 0.01$). In the present work, we adopt a simple finite-difference approach. As for the reaction–diffusion model Eq. (33), we adopted a three-points finite difference approximation of the Laplacian operator. The resulting set of ODEs has been integrated by means a fourth-order Runge–Kutta algorithm, thus obtaining a system of $n = 2N$ ODEs in the 2 N variables $\{u_i\}_{i=1}^{N}$ and $\{v_i\}_{i=1}^{N}$, with $N = 31$.

For low and high values of D, the system stabilizes onto ignited and extinguished steady states, respectively. Intermediate values of D correspond to operating conditions that allow competition between the tendency to ignition due to the nonlinear kinetics, and the extinguishing behavior at the boundaries. This induces complex oscillations and intermittent bursting in the center of the spatial domain.

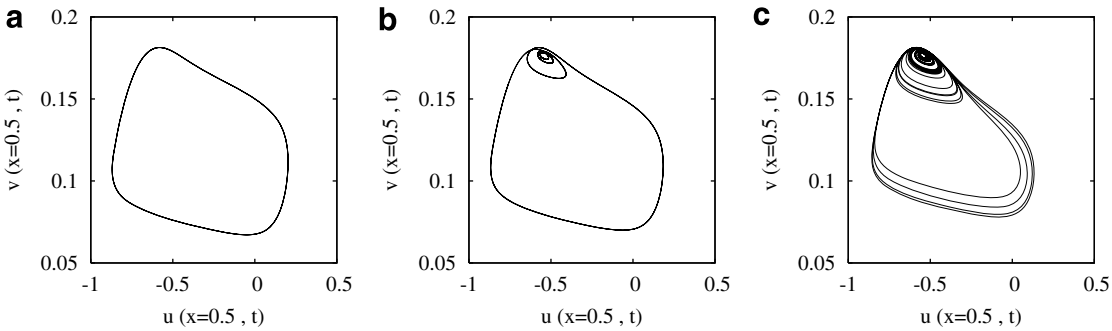

Fig. 7. Two-dimensional projection of the phase-space portrait $v(x = 1/2, t)$ vs $u(x = 1/2, t)$ of the asymptotic behavior of the EA reaction–diffusion model ($n = 62$ ODEs) for three different values of D: (a) $D = 0.0320$, period-one limit cycle; (b) $D = 0.03224$, period-four limit cycle; (c) $D = 0.03228$, chaotic attractor.

Figs. 7(a)–(c) show the two-dimensional projection of the phase-space portrait $v(x = 1/2, t)$ vs $u(x = 1/2, t)$ of the asymptotic behavior of the Arneodo–Elezgaray reaction–diffusion model for three different values of D, corresponding to a period-one limit cycle ($D = 0.0320$), a period-four limit cycle ($D = 0.03224$) and a chaotic attractor ($D = 0.03228$).

Figs. 8–10 display the dynamics and the stretching properties of the EA model for several values of dimensionless diffusivity D giving rise to the attractors depicted in Fig. 7. Specifically, panels(a) depict the time behavior of the concentration at the mid-points, panels(b) the time evolution of the tangential stretching rate, and panels(c) the number of active modes N_{loc}. According to the local normal hyperbolicity assumption the number of active modes N_{loc} (solid lines) is given by $N_{\mathrm{loc}} = N_v + 1$, where N_v is the number of normal stretching rates $\omega_{v,h}$ such that $\omega_{v,h} \geqslant \omega_\tau, h = 1, \ldots, N_v$. In the same panels, N^+, i.e. the number of tangential and normal directions characterized by positive stretching rates, is also depicted (dashed lines).

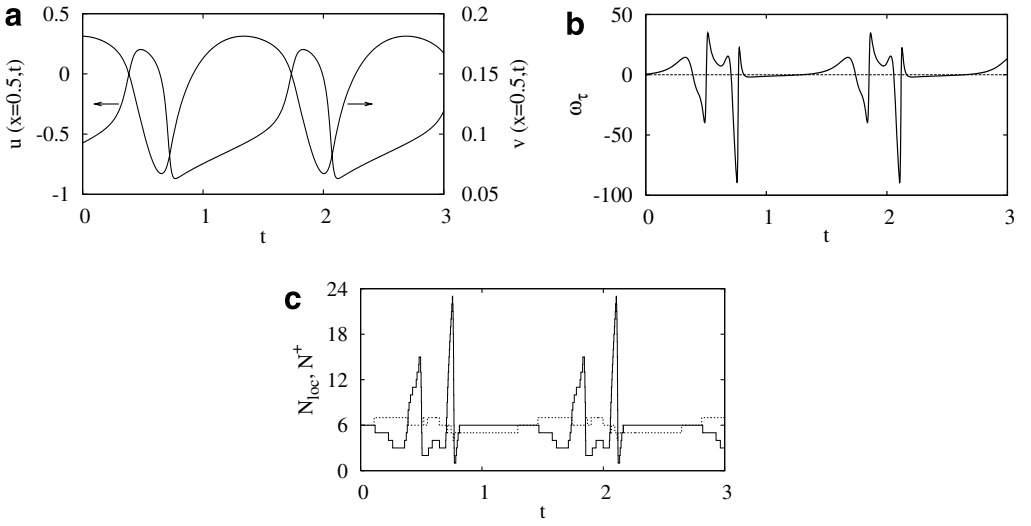

Fig. 8. EA reaction–diffusion model ($n = 62$ ODEs) at $D = 0.0320$ (period-one limit cycle): (a) $u(0.5, t)$ and $v(0.5, t)$ vs t; (b) ω_τ vs t along the system trajectory; (c) N_{loc} (solid line) and N^+ (dashed line) vs t along the system trajectory.

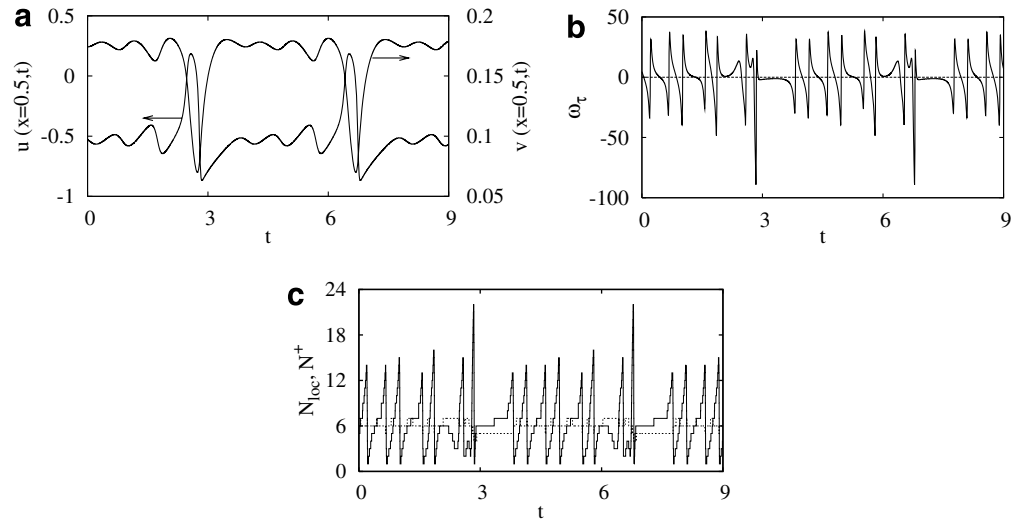

Fig. 9. EA reaction–diffusion model ($n = 62$ ODEs) at $D = 0.03224$ (period-four limit cycle): (a) $u(0.5, t)$ and $v(0.5, t)$ vs t; (b) ω_τ vs t along the system trajectory; (c) N_{loc} (solid line) and N^+ (dashed line) vs t along the system trajectory.

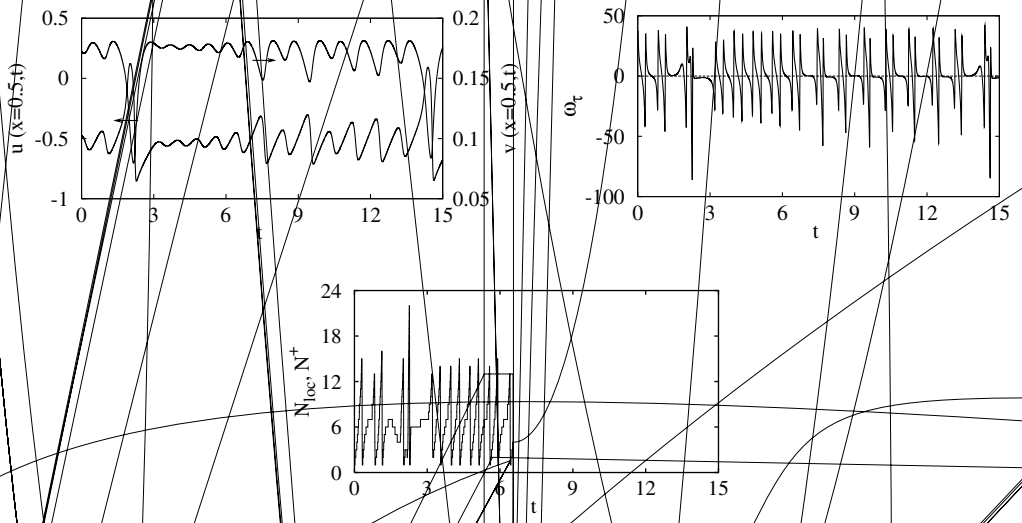

In all these three cases, a peak in the number of active (relevant) modes occurs whenever the tangent stretching rate exhibits a sudden decrease and attains very low negative values. Since ω_τ defines locally the relevant characteristic time scale, a decrease of ω_τ implies that many normal modes becomes locally active (relevant). On the contrary, the number of modes associated with positive (unstable) stretching rates N^+ is practically constant along the system trajectories and oscillates between 5 and 7. This corresponds to the fact that the number of positive pseudo-Lyapunov normal exponents N^+_{pL} equals 5 in all the three cases analyzed. These results will be further discussed in Section 5, in connection with the application of the stretching-based reduction method.

5. The stretching-based reduction method

This Section addresses an embedding-type approach to model reduction based on the stretching characterization of local dynamics.

Stretching-based analysis provides an alternative approach to model reduction, which is more closely related to local embedding methods, addressed e.g. by Robinson in Chapter 16 of his monograph [24]. Essentially, the rationale underlying the results and the "utopian theorems" sketched by Robinson consists in that the computational shortcomings of inertial manifold theory [23,26–28], as well as of any reduction theory relying on the explicit representation of the "relevant" (slow, inertial) invariant manifold as a huge system of nonlinear equations of state[12] could be circumvented by attempting to find a global linear embedding containing the global attractor $\mathscr{A}$. The dimension of the embedding should be close to the Takens' limit $m = \lfloor 2\dim_H(\mathscr{A}) + 1 \rfloor$ [61], where $\dim_H(\mathscr{A})$ is the Hausdorff dimension of the global attractor $\mathscr{A}$, and $\lfloor \alpha \rfloor$ is the upper integer of α.

The Robinson scientific program to model reduction consists of three main requisites: (i) linear embedding of the dynamics, which is (ii) globally defined, and (iii) possesses the smallest possible dimension compatible with Takens' and Whitney's embedding theorems [61]. We shall see below that the application of stretching-based analysis to the problem of model reduction provides a way to meet some of these requirements.

Let $\mathbf{x}_0$ be a point along a system trajectory at time $t = t_0$. Stretching-based analysis at point $\mathbf{x}_0$ defines the actual driving time scale $t_c(\mathbf{x}_0)$ as the reciprocal of the tangential stretching rate $t_c(\mathbf{x}_0) = [\omega_\tau(\mathbf{x}_0)]^{-1}$ associated with the central direction $\hat{\mathbf{f}}(\mathbf{x}_0)$. It further defines an ordered system of mutually orthogonal directions $\hat{\mathbf{n}}_h(\mathbf{x}_0), h = 1, \ldots, n-1$, normal to $\hat{\mathbf{f}}(\mathbf{x}_0)$ and associated with the local directions of maximum stretching. The characteristic time scales $t_{v,h}(\mathbf{x}_0)$ associated with the evolution of the normal perturbations are given by the reciprocal of the normal stretching rates,

$$t_{v,h}(\mathbf{x}_0) = \frac{1}{\omega_{v,h}(\mathbf{x}_0)}, \quad h = 1, \ldots, n-1 \tag{41}$$

Observe that these time scales possess a sign, i.e. they can attain both positive and negative values. A negative value for $t_{v,h}(\mathbf{x}_0)$ indicates that the corresponding normal perturbation decays, while a positive value corresponds to a locally unstable normal perturbation.

By adopting the criterion deriving from local normal hyperbolicity analysis, the relevant directions for expressing local system dynamics in the neighborhood of $\mathbf{x}_0$ are those associated with the central direction itself $\hat{\mathbf{f}}$, and with the first $N_{\mathrm{loc}} - 1$ normal perturbations, as in the condition Eq. (32). This criterion expresses quantitatively the intuitive observation that the relevant directions in the neighborhood of $\mathbf{x}_0$ are those associated with normal perturbations that are either slower or more unstable than the driving central time scale.

Let us indicate with $\hat{\mathbf{e}}_1(\mathbf{x}_0) = \hat{\mathbf{f}}(\mathbf{x}_0)$, $\hat{\mathbf{e}}_2(\mathbf{x}_0) = \hat{\mathbf{n}}_1(\mathbf{x}_0), \ldots, \hat{\mathbf{e}}_{N_{\mathrm{loc}}}(\mathbf{x}_0) = \hat{\mathbf{n}}_{N_{\mathrm{loc}}-1}(\mathbf{x}_0)$ the unit vectors associated with the first N_{loc} modes. In the neighborhood of $\mathbf{x}_0$, one can approximate the state vector $\mathbf{x}(t)$ as

$$\mathbf{x}(t) = \mathbf{x}_0 + \sum_{h=1}^{N_{\mathrm{loc}}} \xi_h(t)\hat{\mathbf{e}}_h(\mathbf{x}_0) \tag{42}$$

where $\xi_h(t), h = 1, \ldots, N_{\mathrm{loc}}$, represents the local coordinates of a local linear embedding close to $\mathbf{x}_0$. Substituting Eq. (42) into system dynamics Eq. (3) yields

$$\sum_{h=1}^{N_{\mathrm{loc}}} \frac{\mathrm{d}\xi_h}{\mathrm{d}t}\hat{\mathbf{e}}_h(\mathbf{x}_0) = \mathbf{f}\left(\mathbf{x}_0 + \sum_{h=1}^{N_{\mathrm{loc}}} \xi_h\hat{\mathbf{e}}_h(\mathbf{x}_0)\right) \tag{43}$$

which can be explicited with respect to $\mathrm{d}\xi_k/\mathrm{d}t$ by taking the inner product with respect to $\hat{\mathbf{e}}_k(\mathbf{x}_0)$ and enforcing the orthonormality of this vector system,

$$\frac{\mathrm{d}\xi_k}{\mathrm{d}t} = \hat{\mathbf{e}}_k(\mathbf{x}_0) \cdot \mathbf{f}\left(\mathbf{x}_0 + \sum_{h=1}^{N_{\mathrm{loc}}} \xi_h\hat{\mathbf{e}}_h(\mathbf{x}_0)\right), \quad k = 1, \ldots, N_{\mathrm{loc}} \tag{44}$$

The initial conditions on the local coordinates are

$$\xi_k(t = t_0) = 0, \quad k = 1, \ldots, N_{\mathrm{loc}} \tag{45}$$

The validity of Eq. (44) is intrinsically local, i.e. Eq. (44) applies in a small neighborhood of $\mathbf{x}_0$. The analysis of the local time scales provides a quantitative estimate for the size of this neighborhood. Let $T_{\min} = \min_{h=1}^{N_{\mathrm{loc}}(\mathbf{x}_0)-1}\{|t_\tau|, |t_{v,h}|\}$ the minimum time scale amongst the relevant N_{loc} modes. Eq. (44) represents a valid approximation for the local dynamics in the interval $t \in [t_0, t_1)$ which is of order of magnitude of $T_{\min}$, i.e.

$$t_1 - t_0 = cT_{\min}, \quad c \sim \mathcal{O}(1) \tag{46}$$

where c is a constant of unit order of magnitude. In practical applications we chose $c \in [0.5, 2]$.

The Stretching-Based Reduction method (SBR for short) consists in the repeated application of the procedure expressed by the following linear embedding:

$$\begin{aligned}
&\mathbf{x}(t) = \mathbf{x}_\alpha + \sum_{h=1}^{N_{\mathrm{loc},\alpha}} \xi_h^{(\alpha)}(t)\hat{\mathbf{e}}_h^{(\alpha)}(\mathbf{x}_\alpha), \quad t \in [t_\alpha, t_{\alpha+1}),\ \alpha = 0, 1, 2,\\
&\frac{\mathrm{d}\xi_k^{(\alpha)}}{\mathrm{d}t} = \hat{\mathbf{e}}_k^{(\alpha)}(\mathbf{x}_\alpha) \cdot \mathbf{f}\left(\mathbf{x}_\alpha + \sum_{h=1}^{N_{\mathrm{loc},\alpha}} \xi_h^{(\alpha)}\hat{\mathbf{e}}_h^{\alpha}(\mathbf{x}_\alpha)\right) = g_k^{(\alpha)}(\boldsymbol{\xi}^{(\alpha)}), \quad k = 1, \ldots, N_{\mathrm{loc},\alpha} \quad \xi_k^{(\alpha)}(t = t_\alpha) = 0,\\
&t_{\alpha+1} = t_\alpha + cT_{\min}(\mathbf{x}_\alpha)
\end{aligned} \tag{47}$$

where α is the counter in the repeated application of the procedure, $N_{\mathrm{loc},\alpha}$ is the number of relevant local direction at $\mathbf{x}_\alpha$, and $\mathbf{x}_0, \mathbf{x}_1, \ldots \mathbf{x}_\alpha, \ldots$ are the endpoints of system orbits at the time instants t_α corresponding to the switching from a local coordinate chart to the next.

The SBR method is, therefore, a local linear embedding method of the system's dynamics whereby solely the most unstable/slow directions, compared with the relevant time scale, are considered. A local coordinate system is established along the trajectory, under the assumption that the system's evolution is confined into the span of the first N_{loc} modes, including the central direction of the initial point.

It is clear that such reduction procedure is particularly simple as it does not require the use of any equation of state, involving exclusively the integration of a reduced system of $N_{\mathrm{loc},\alpha}$ ordinary differential equations for the local coordinates $\xi_1^{(\alpha)}, \ldots, \xi_{N_{\mathrm{loc},\alpha}}^{(\alpha)}$. Therefore, this reduction procedure can be applied starting from a generic point of the phase space. This means that it is absolutely not necessary that the initial condition be on a slow manifold of some dimension.

5.1. Stiffness elimination

Classical simplification/reduction methods for complex chemical kinetics (ILDM or CSP) can be used to eliminate stiffness by pruning the stiff components of the kinetics. Whenever model dynamics collapses onto a lower-dimensional manifold, the exhausted fast modes, which are responsible for numerical stiffness, are rejected, by projecting the dynamics onto the slower modes which describe the structure of the approximate slow-dimensional manifold.

The SBR method also provides stiffness elimination, by confining local dynamics onto a lower-dimensional linear embedding corresponding to the actual driving time scale (associated with the central direction) and to the most unstable/slow time scales with respect to the central one. In order to ascertain this issue, it is convenient to consider a simple prototypical three-dimensional linear system $\dot{\mathbf{x}} = \mathbf{A}\mathbf{x}$, where the matrix $\mathbf{A}$ is given by

$$\mathbf{A} = \begin{pmatrix} -1 & -2 & 1 \\ 0 & -10 & 4 \\ 0 & 0 & -1000 \end{pmatrix} \tag{48}$$

This linear system is characterized by three negative eigenvalues $\lambda_1 = -1, \lambda_2 = -10, \lambda_3 = -100$, and a significant gap (one/two orders of magnitude exists between consecutive time scales).

Fig. 11(a) depicts the behavior of the tangential (bold solid line), and normal stretching rates (dashed lines) with reversed sign along the system orbit obtained from the reduced SBR model of the linear system Eq. (48). As expected $-\omega_\tau$ progressively decreases and crosses first $-\omega_{v,1}$, at a time instant $t_1 \simeq 10^{-2} \sim \mathcal{O}(-\lambda_3^{-1})$ and subsequently $-\omega_{v,2}$ at a time instant $t_2 \sim \mathcal{O}(-\lambda_2^{-1})$. This means that the relevant driving time scale expressed by $-1/\omega_\tau$, decreases progressively along system orbit. Correspondingly, the number of relevant modes N_{loc} detected by the SBR method decreases from $N_{\mathrm{loc}} = 3$, at the beginning of the trajectory, up to $N_{\mathrm{loc}} = 1$, when only the dominant mode associated with $\lambda_1 = -1$ becomes significant.

A stiffness ratio can be defined as $R_{\mathrm{stiff}} = \omega_\tau/\omega_{v,N_{\mathrm{loc}}-1}$, whenever $N_{\mathrm{loc}} \geqslant 2$. Of course the reduced system ceases to be stiff if $N_{\mathrm{loc}} = 1$. Consequently, the progressive decrease of both $-\omega_\tau$ and N_{loc} depicted in Fig. 11(a) and (b) indicates that the SBR method provides an effective stiffness reduction in the model equation, obtained by simply discarding the fastest normal modes from the local linear embedding.

As a further confirmation we analyze the eigenvalues $\{\zeta_i\}_{i=1}^{N_{\mathrm{loc}}}$ of the $N_{\mathrm{loc}} \times N_{\mathrm{loc}}$ Jacobian $\mathbf{J}^{R,(\alpha)} = J_{k,j}^{R,(\alpha)}$ of the SBR reduced model Eq. (47):

$$J_{k,j}^R(\mathbf{x}) = \frac{\partial g_k(\boldsymbol{\xi}^\alpha)}{\partial \xi_j^{(\alpha)}} = \sum_{m=1}^{n}\sum_{p=1}^{n} \widehat{e}_{k,m}(\mathbf{x}) J_{m,p}(\mathbf{x}) \widehat{e}_{j,p}(\mathbf{x}), \quad k,j = 1,\ldots,N_{\mathrm{loc},\alpha} \tag{49}$$

where $J_{m,p} = \partial f_m/\partial x_p$ and $\mathbf{x}(t) = \mathbf{x}_\alpha + \sum_{h=1}^{N_{\mathrm{loc},\alpha}} \xi_h^{(\alpha)}(t)\hat{\mathbf{e}}_h^{(\alpha)}(\mathbf{x}_\alpha)$, along the system trajectory. Fig. 11(c) shows the eigenvalues of $\mathbf{J}^{R,(\alpha)}$ for the linear system under investigation confirming that, for $N_{\mathrm{loc}} = 2$, the ratio of the largest to the lowest eigenvalue for the SBR model is reduced by two decades with respect to the original system. Stiffness elimination implies that the reduced model Eq. (47) can be numerically integrated by explicit methods

and that the integration time-step is actually controlled by the accuracy required for the solution in the time interval $[t_\alpha, t_{\alpha+1})$.

5.2. Different criteria for the dimension of the linear embedding

Let us further address the definition of practical criteria for the estimate of the number of relevant directions spanning the local linear embedding.

The first criterion (already considered) may be referred to as the Local Normal Hyperbolicity criterion (LNH) and stems from the application of normal hyperbolicity concepts at a local level: it assumes N_{loc} as the number of relevant directions (i.e. the central direction plus the normal directions that are slower/more unstable than the central direction). In so doing, the "embedding subspace" of dimension N_{loc} may be considered as a locally normally hyperbolic embedding manifold.

For systems possessing nontrivial limit sets (such as limit cycles, chaotic attractors, etc.), it is possible to provide other criteria, namely to choose the number of relevant directions forming the local linear embedding as N^+, i.e. as the central direction plus all the normal directions which are associated with positive stretching rates. This criterion will be referred to as the Local Unstable Mode (LUM) criterion.

To give an example, Fig. 12 depicts the $x-z$ projection of the reconstructed SBR attractor obtained by enforcing the LNH criterion (panel A), and the LUM criterion (panel B) for the Lorenz system. In the latter case $N^+ = 2$ uniformly throughout the chaotic trajectory.

Both criteria provide a satisfactory reconstruction of the chaotic attractor for the Lorenz system (compare Figs. 12(a) and (b) with Fig. 5(a)). Fig. 12(c) shows the behavior of N_{loc} along a chaotic trajectory on the limit attractor. For almost all the time instants, $N_{\mathrm{loc}} = 2$, with the exception of few localized spikes at which $N_{\mathrm{loc}} = 3$. These spikes correspond to the time intervals at which $\omega_{v,2} > \omega_\tau$, observed in Fig. 5(b).

In the case of dynamical systems confined to periodic or chaotic attractors, it is possible to provide an alternative criterion, consisting in choosing the relevant modes for the local dynamics as those directions that are locally associated with nonnegative pseudo-Lyapunov exponents. Let N^+_{pL} be the (constant) number of such

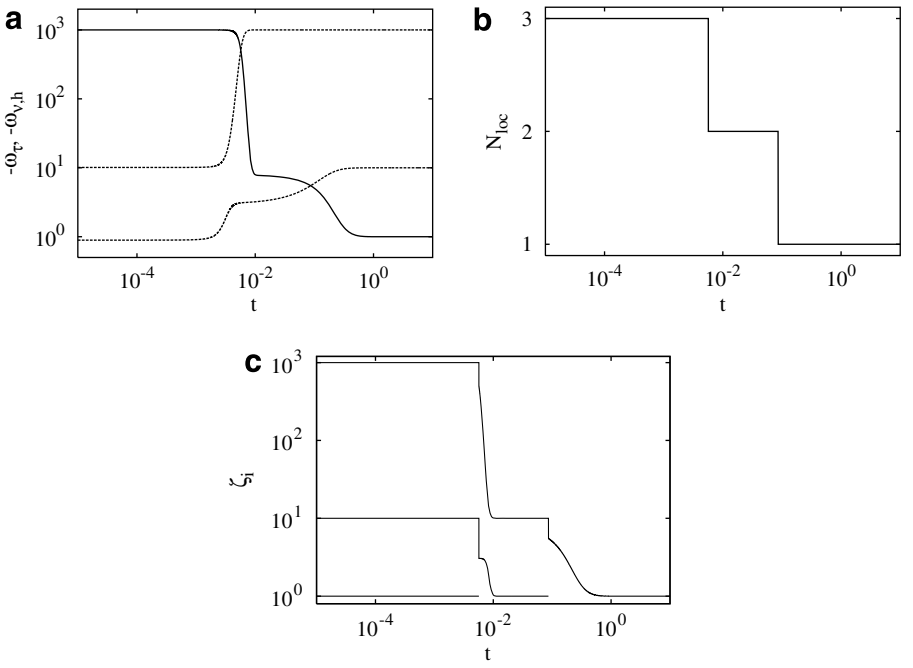

Fig. 11. (a) Tangential (bold line) and normal stretching rates (dotted lines) with reversed sign as a function of time t along the system orbit obtained from the reduced SBR model of the linear system Eq. (48). Starting point $\mathbf{x}_0 = (100, 20, 70)$. (b) Behavior of N_{loc} vs t for the same orbit. (c) Eigenvalues $\{\zeta_i\}_{i=1}^{N_{\mathrm{loc}}}$ of the Jacobian $\mathbf{J}^{R,(\alpha)}$ of the reduced SBR model along the same orbit.

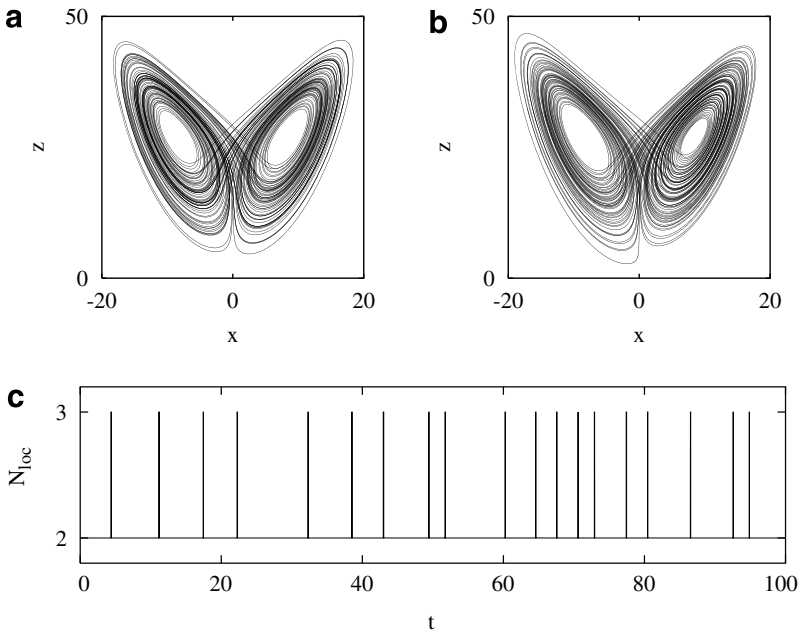

Fig. 12. (a) SBR reconstruction of the Lorenz attractor, using the Local Normal Hyperbolicity criterion (LNH). The number of modes N_{loc} along a system trajectory is depicted in panel (c). (b) SBR reconstruction of the Lorenz attractor, using the Local Unstable Mode criterion (LUM). In this case $N^+ = 2$. (c) N_{loc} vs t for the SBR reconstruction depicted in panel (a).

modes. In this case, the relevant modes are locally $\widehat{f}(\mathbf{x}_0)$ and the first $N^+_{\mathrm{pL}} - 1$ normal modes associated with nonnegative values of $\Lambda_{v,h}, h = 1, \ldots, N^+_{\mathrm{pL}}$. This criterion will be referred to the the Pseudo Lyapunov Unstable Mode (PLUM) criterion.

A detailed numerical analysis of the SBR method applied to PDEs and adopting the criteria described above is developed in Sections 5.3 and 5.4. However, a general comparison of these three (LNH, NUM, PLUM) criteria follows readily from their definitions.

The LNH criterion is certainly the safest of the three, and applies on equal footing for dynamical systems relaxing towards an equilibrium point, or evolving within a nontrivial (periodic, chaotic) limit set. It is certainly the most conservative criterion in terms of the number of relevant modes, since $N_{\mathrm{loc}}(\mathbf{x}_0)$ is generally greater than $N^+(\mathbf{x}_0)$ or N^+_{pL} (see e.g. Figs. 8–10).

In the case of dynamical systems converging towards a stable equilibrium point, $N_{\mathrm{loc}}(\mathbf{x}_0)$ may be greater than 1, even close to equilibrium. This is due to the fact that even in constant-coefficient linear dynamical systems, the coefficient matrix of which possesses all the eigenvalues with negative real part, some of the normal stretching rates along system trajectories may be eventually positive, expressing the occurrence of a local growth in the dynamics of normal perturbations.

The NUM and PLUM criteria apply to the dynamic evolution within periodic/chaotic attractors. The NUM criterion is more restrictive than PLUM, and can be applied along system orbits without any a priori knowledge of system dynamics. On the contrary, PLUM criterion requires a priori information on the spectrum of pseudo-Lyapunov exponents. Generically, $N^+(\mathbf{x}_0) \geqslant N^+_{\mathrm{pL}}$, and, therefore, PLUM requires the local integration of fewer variables. Both in NUM and PLUM criteria, the interval of validity of each local coordinate chart is controlled by the reciprocal of the absolute value of the maximum stretching rate amongst the vectors spanning the linear embedding.

To conclude this Section, we are able to comment the analogy between the SBR method and the Robinson scientific project outlined at the beginning of this Section. With respect to the three main points of this program, the SBR method provides: (i) an approximate linear embedding, (ii) which holds locally and not globally, and such that (iii) the dimension of each local coordinate chart is greater than the Takens limit. Empirical

observations on several systems of PDE, indicate that for the dynamics confined onto the limit sets, the dimension of each local linear embedding is of the order of the Takens limit [45].

Although there are intrinsic differences between SBR and the "utopian" embedding program envisaged by Robinson (which can be viewed as the *perfect* reduction method still to be figured out both in theory and in practice), SBR provides a realistic and easy-to-implement strategy for model reduction of generic dynamical systems, attempting to conform to this program.

5.3. PDE example I: the EA system

The EA reaction diffusion system described in Section 4.3 provides a valid model case to test the performance of the SBR method. Fig. 13 shows the time behavior of the averaged normal stretching rates along an orbit lying on the limit attractor of the EA system for $D = 0.03228$. For large t, this averages saturates to the corresponding normal pseudo-Lyapunov exponent. The number of positive pseudo-Lyapunov exponents is $N^+_{\mathrm{pL},v} = 5$ so that $N^+_{\mathrm{pL}} = 6$ (since the central direction corresponding to $\Lambda_\tau = 0$ should be included as well). Throughout the range of diffusivities considered, we found $N^+ = 6$ uniformly.

Consider the SBR method by enforcing the PLUM criterion. This choice determines the smallest number of relevant local modes within each linear embedding, compared with NLH and NUM strategies.

As noted, the dimension of each local embedding is $N^+_{\mathrm{pL}} = 6$ uniformly, although each local basis changes orientation. Within each local basis (i.e. for a fixed value of the counter α entering Eq. (47)), the reduced system has been integrated by applying the fourth-order explicit Runge–Kutta integration algorithm for a time horizon given by Eq. (46).

Fig. 14 shows the quantitative agreement between the trajectories of the original (full) system and of the SBR model in the presence of limit cycles in the dynamics.

In the case of chaotic attractors, it is meaningless to perform a trajectory-based comparison, which should retain validity solely for short time intervals compared with the maximum Lyapunov exponent of the system. Instead, it is useful to consider global reconstruction properties, which can be qualitatively verified by analyzing the phase plot of the limit attractor, as shown in Fig. 15 for the original (full) system (left panel) and the SBR model (right panel).

5.4. PDE example II: diffusive-thermal instabilities in planar flames

Another challenging PDE test is represented by a diffusive-thermal model for planar flames. Premixed flames with one-step chemistry can exhibit a variety of instabilities giving rise to rich dynamical behaviors. Depending on the value taken by model parameters, such as the Lewis number Le, measuring the ratio of thermal to mass diffusivity of the limiting (deficient) reactant, the flame can display cellular conformations (i.e. departing from the planar solution) and/or pulsations [62]. Linear stability analyses [63] (as well as nonlinear

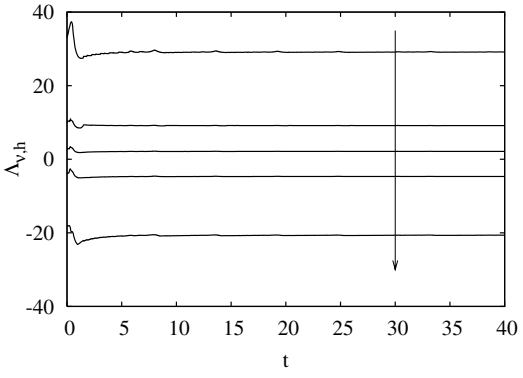

Fig. 13. Analysis of the EA reaction–diffusion model at $D = 0.03228$ (chaotic attractor). Time behavior of $\langle \omega_{v,h}(\mathbf{x}(t)) \rangle$ along an orbit of the EA reaction diffusion model. The arrow indicates the direction of increasing $h = 1, 3, 5, 7, 9$.

Fig. 14 ced mo
(contin ne: ori
four li e.

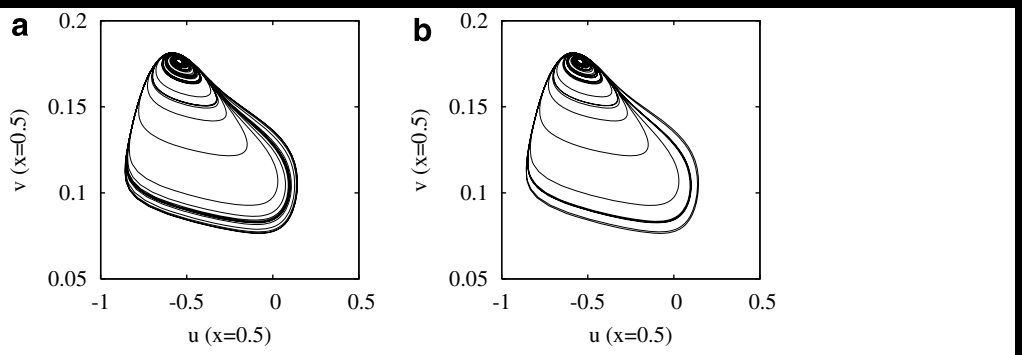

Fig. 15. EA reaction–diffusion system in chaotic regime, $D = 0.03228$: (a) original system; (b) reduced model using PLUM criterion for a number of relevant directions equal to $N_{pl} = 6$.

analys
verse
hydr
puls
mo
ter

$$\begin{aligned}\partial_t\theta + v_f(t)\partial_x\theta &= \partial_x^2\theta + \omega(\theta, Y)\\ \partial_t Y + v_f(t)\partial_x Y &= Le^{-1}\partial_x^2 Y - \omega(\theta, Y)\end{aligned} \tag{50}$$

where the dimensionless reaction rate is given by

$$\omega(\theta, Y) = \frac{Ze^2}{2Le} Y \exp\left(-\frac{Ze(1-\theta)}{1-\alpha(1-\theta)}\right) \tag{51}$$

The dimensionless groups entering Eq. (50) are: the Lewis number Le, the dimensionless activation energy Ze also referred to as the Zeldovich number, and $\alpha = (T_b - T_u)/T_b$. The flame speed $v_f(t)$ can be defined as $v_f = \int_\Omega \omega \mathrm{d}x$.

Following [66], initial conditions are set equal to the $Ze \to \infty$ solution, i.e. $\theta(x,0) = 1$ and $Y(x,0) = 0$ for $x \in (0, \ell]$ and $\theta(x,0) = \mathrm{e}^x$ and $Y(x,0) = 1 - \mathrm{e}^{xLe}$ for $x \in [-\ell, 0]$. Dirichlet boundary conditions, compatible with the given initial conditions provided ℓ is sufficiently large, are set at the inflow boundary, $\theta(-\ell, t) = 0$ and $Y(-\ell, t) = 1$, and zero flux conditions at the outflow boundary.

Eq. (50) was integrated in time using DVODE (with a time horizon as in Eq. (46) with $c = 1$) and applying a second-order finite volume discretization (see [67]) on a $N = 64$ cells fixed nonuniform grid, refined locally around $x = 0$ so as to accommodate enough cells within the flame thickness. The discretized system of PDEs Eq. (50) results into a system of $2N = 128$ ODEs of the form Eq. (3) in the variables $\{\theta_i\}_{i=1,N}$ and $\{Y_i\}_{i=1,N}$. Henceforth we set $Le = 4$, and let the Zeldovich number vary in the range $Ze = (10, 13)$. Specifically, we consider three cases, $Ze = 10.2, 11.5, 13$. Periodic solutions (limit cycles) were found for all the three cases, with a period-doubling occurring within the interval $(11.5, 13)$.

The upper portions of Figs. 16(a)–(c) display the flame speeds $v_f(t)$ in the three cases considered. An analysis of the stretching rates along the limit cycles was performed to evaluate, according to the LNH and PLUM criteria, the number of relevant modes N_{loc} and the number of positive pseudo-Lyapunov exponents N^+_{pL}. The

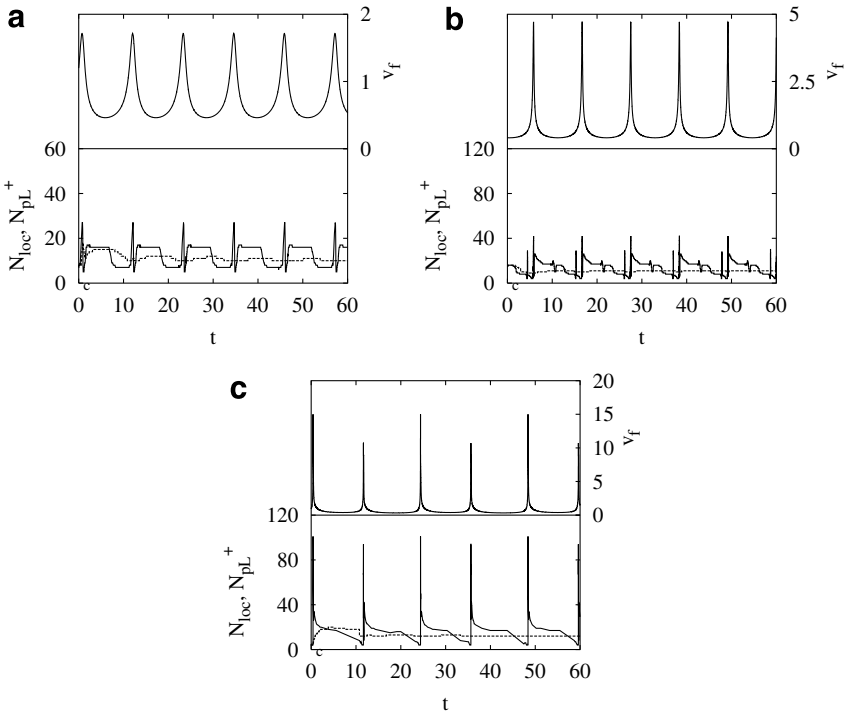

Fig. 16. Upper portion: flame speed $v_f(t)$. Lower portion: $N_{\mathrm{loc}}(t)$ (continuous line), $N^+_{\mathrm{pL}}(t)$ (dotted line). (a) $Ze = 10.2$, (b) $Ze = 11.5$, (c) $Ze = 13.0$.

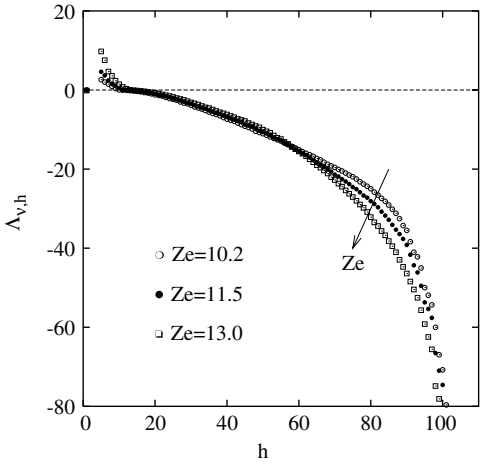

Fig. 17. Spectrum of normal pseudo-Lyapunov numbers $\Lambda_{v,h}$ for the cases considered.

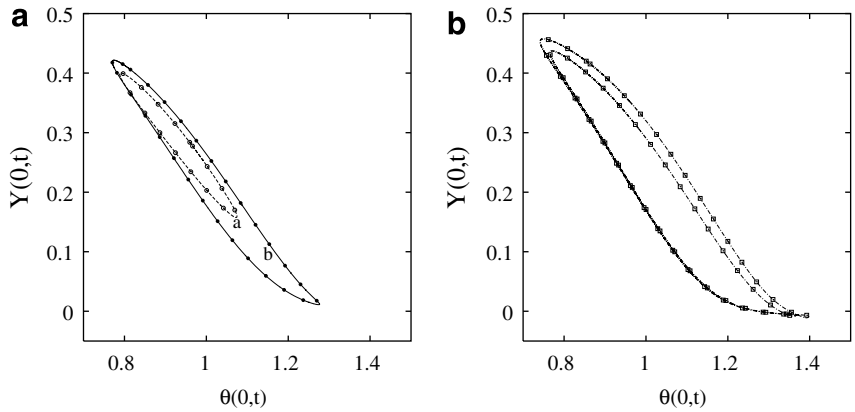

Fig. 18. Phase portrait of mid-field values $\theta(0,t), Y(0,t)$. Symbols refer to the complete solution (○) $Ze = 10.2$, (●) $Ze = 11.5$, (□) $Ze = 13.0$. Continuous curves refer to the SBR reconstructed solutions using PLUM criterion. Panel (a) (curve a) $Ze = 10.2$, $N^+_{\mathrm{pL}} = 10$, (curve b) $Ze = 11.5$, $N^+_{\mathrm{pL}} = 11$, Panel (b) $Ze = 13.0$, $N^+_{\mathrm{pL}} = 14$.

lower portions of Figs. 16(a)–(c) display N_{loc}, which exhibits localized bursts in correspondence of flame speed peaks, together with N^+_{pL} saturating to constant values.

A rather significant diagnostic indicator of the dynamics is the spectrum of pseudo-Lyapunov exponents $\Lambda_{v,h}$ shown in Fig. 17, for $4 \leqslant h \leqslant 100$ (the remaining values falling above and below the shown range[13]). The positive part of the spectrum and in particular the number N^+_{pL} of positive pseudo-Lyapunov numbers represents a measure of the embedding dimension of the attractor of the system which, in the present range of Ze numbers is a limit cycle, i.e. a one-dimensional manifold. In the three cases considered we find $N^+_{\mathrm{pL}} = 10$ at $Ze = 10.2, N^+_{\mathrm{pL}} = 11$ at $Ze = 11.5, N^+_{\mathrm{pL}} = 14$ at $Ze = 13$. It is also significant to note that such values of N^+_{pL} were found to be independent of the number N of discretization cells (provided N is sufficiently large for proper resolution). In other words increasing N leaves the upper (unstable) part of the spectrum unchanged while adding stable modes to the lower part of the spectrum.

The SBR approach was used to reconstruct the solutions using the PLUM criterion, i.e. a number of modes equal to the value of N^+_{pL}, which corresponds to roughly 10% of the original 128 modes (see the dotted lines in

[13] The following maximum normal pseudo Lyapunov exponents were found: $\Lambda_{v,1} \approx 30830$ at $Ze = 10.2$, $\Lambda_{v,1} \approx 31526$ at $Ze = 11.5$, $\Lambda_{v,1} \approx 32048$ at $Ze = 11.5$.

Fig. 16(a)–(c)). Fig. 18(a) and (b) display the result of such reconstruction for the three values of the Zeldovich number. The actual solutions and the reconstructed solutions are virtually indistinguishable, this in spite of $N_{\mathrm{loc}}(t)$ being even far greater than N_{pL}^{+}, albeit only locally, during the periodic bursts of flame instability (see Fig. 16).

The results of the present section and of Section 5.1 indicate that the SBR method, implemented on PDEs even with the more "loose" mode selection criterion (namely PLUM) is able to provide a significant mode reduction with an excellent quantitative and qualitative agreement in the evolution of the state variables and in the reconstruction of the limit sets, both in chaotic and periodic conditions.

6. Concluding remarks

Local normal stretching rate analysis provides a simple and geometrically meaningful way to characterize the instabilities and the time scales associated with normal perturbations compared to tangential dynamics along a given manifold (orbit).

Starting from normal stretching rate analysis, a reduction method (SBR) has been developed, which makes use of a local linear embedding of the dynamics with respect to a local coordinate chart associated with the most unstable and/or slow normal stretching directions compared to the driving dynamic time scale.

The SBR method provides a simple and very promising reduction approach that applies both to large systems of ODEs or to systems of PDEs. In the case of reaction/diffusion model, the SBR approach considers the reaction/diffusion operator as a single entity and does not perform any conceptual decoupling between the reaction/diffusion time scales [22]. This makes it possible to achieve a significant reduction efficiency, as described in connection with chaotic reaction/diffusion models and premixed oscillating flames.

The SBR method handles on equal footing relaxation dynamics towards an equilibrium point and asymptotic periodic/chaotic oscillations.

The numerical examples described in this article indicate that local linear embedding methods provide an effective alternative to other methods of model reduction based on the explicit solution of the equations of state for the approximate slow/inertial manifold. Future research will address the assessment of the computational efficiency of this approach in forms of accuracy and optimization of the critical numerical aspects. Two numerical/computational aspects should be investigated in detail: (i) specific integration methods for the set of ODEs representing the dynamics of the local coordinates $\xi_1^{(\alpha)}, \ldots, \xi_{N_{\mathrm{loc},\alpha}}^{(\alpha)}$ and, (ii) possible alternative and improved criteria for estimating the time interval $[t_\alpha, t_{\alpha+1}]$ of validity of each local coordinate chart.

Appendix A. The role of conservation laws

The dynamic behavior of systems arising from chemical kinetic modelling is often characterized by the occurrence of conservation laws that enforce stoichiometric constraints, which may depend on the initial conditions. Therefore, the phase space of these systems is foliated with an uncountable family of lower-dimensional stoichiometric manifolds. For a fixed combination of the initial conditions, system orbits lie on one of these stoichiometric manifolds [68].

In order to clarify the role of conservation laws within the stretching-based approach, the classical Michaelis–Menten model for a simple enzymatic reaction in a batch system is considered: $E + S \rightleftharpoons ES, ES \rightarrow E + P$, where E, S, ES an P are the enzyme, the substrate, the enzyme–substrate complex, and the final product of the reaction, respectively. Since the dynamics of product formation is decoupled from the remaining kinetic scheme, the Michaelis–Menten model gives rise to a system of three ordinary differential equations

$$\begin{aligned} \dot{x}_S &= -k_1 x_E x_S + k_{-1} x_{ES} \\ \dot{x}_{ES} &= k_1 x_E x_S - (k_1 + k) x_{ES} \\ \dot{x}_E &= -k_1 x_E x_S + (k_1 + k) x_{ES} \end{aligned} \tag{A.1}$$

where x_S, x_{ES} and x_E are the substrate, enzyme complex, and free enzyme concentrations, respectively, and k_1, k_{-1}, k the kinetic rate coefficients.

The three-dimensional system Eq. (A.1) admits a two-dimensional slow invariant manifold $\mathscr{W}_2$, depicted in Fig. A.1 which, for small values of the ratio $x_{E,0}/x_S(0), x_{E,0} = x_E(0) + x_{ES}(0)$ being the total initial enzyme concentration, is well approximated by the quasi-steady state result $x_{ES} = x_E x_S/K_M$, where $K_M = (k_{-1} + k)/k_1$ is the Michaelis–Menten constant.

The system Eq. (A.1) is characterized by the conservation law

$$x_E(t) + x_{ES}(t) = x_{E,0} \tag{A.2}$$

expressing enzyme conservation in all of its forms, i.e. either as a free enzyme or bound to the substrate to form the complex *ES*. Of course, this conservation law can be enforced by directly substituting it within Eq. (A.1), e.g. expressing x_E as a function of x_{ES} and $x_{E,0}$. In this way, a two-dimensional system is obtained, in which the initial condition on the total enzyme concentration enters explicitly into system equations as an additional parameter.

For fixed $x_{E,0}$, the slow invariant manifold of the two-dimensional system so obtained becomes a one-dimensional invariant manifold $\mathscr{W}_1(x_{E,0})$, which corresponds to the intersection of $\mathscr{W}_2$ with the conservation law for the total enzyme Eq. (A.2). Indeed, $\mathscr{W}_2$ can be viewed as a foliated manifold $\mathscr{W}_2 = \bigcup_{x_{E,0}} \mathscr{W}_1(x_{E,0})$, formed by the uncountable family of these one-dimensional manifolds parametrized with respect to $x_{E,0}$.

The result of the stretching rate analysis applied to Eq. (A.1) is depicted in Fig. A.2 (solid lines). While ω_τ and the second normal stretching rate $\omega_{\nu,2}$ are always negative, the first, maximum normal stretching rate $\omega_{\nu,1}$ is positive. This, apparently unexpected result, is a consequence of the fact that stretching rate analysis applied

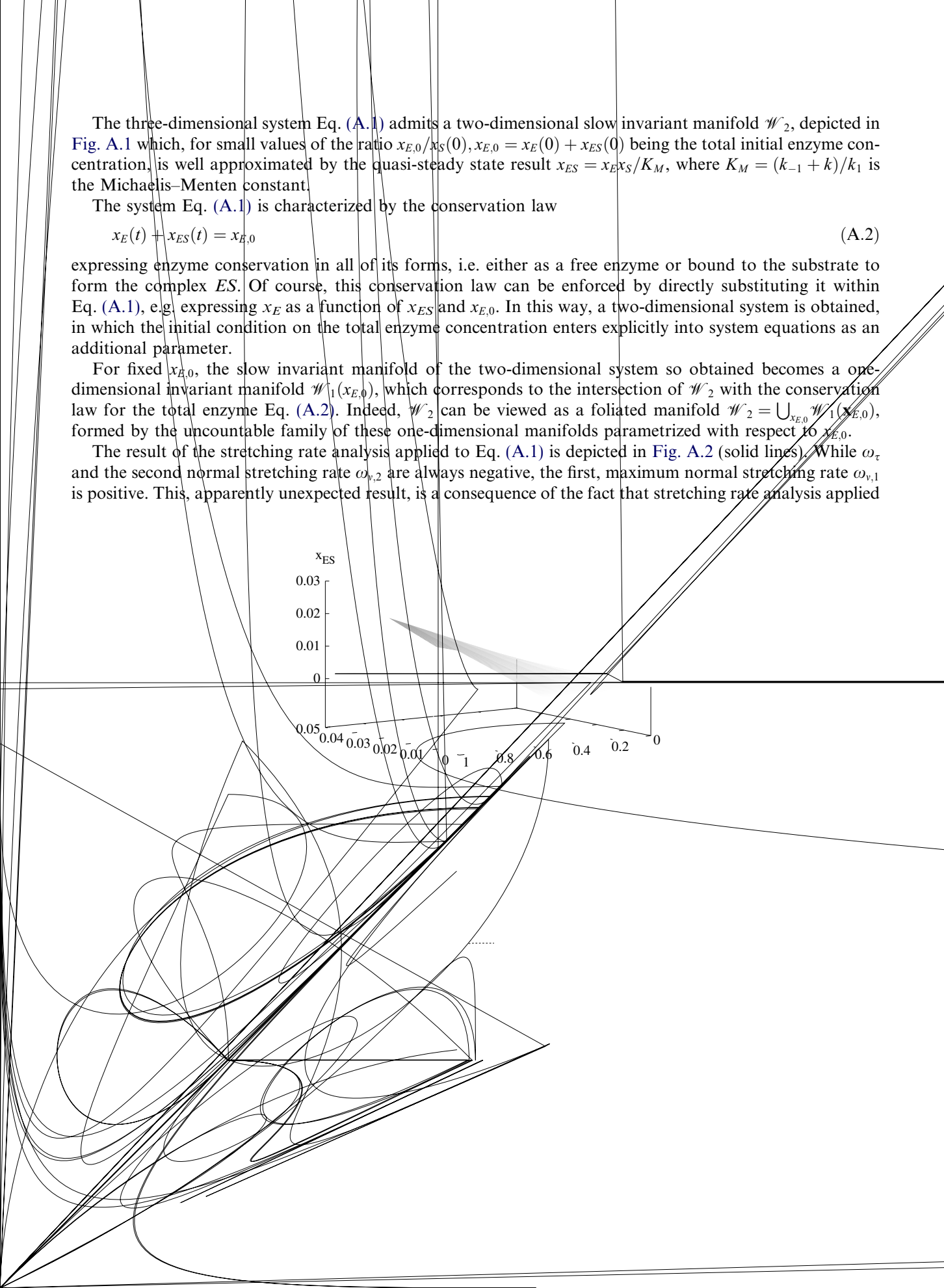

to the three-dimensional system Eq. (A.1) explores and finds the directions of maximum normal stretching in the tangent subspace, which in principle may not satisfy the conservation law imposed on the enzyme concentration. Therefore, stretching analysis yields $N_{\mathrm{loc}} = 2$, which correctly reflects the fact that slow invariant manifold of the three-dimensional system is a two-dimensional structure foliated by one-dimensional slow manifold depending on the initial conditions.

The existence of a direction of positive normal stretching can be further ascertained by means of a simple numerical experiment. Starting from the solution of Eq. (A.1) for $x_S(0) = 1, x_E = x_{E,0} = 0.01$, we pick a point along system the orbit, say $x_S^* = 0.8205, x_E^* = 7.088 \times 10^{-3}, x_{ES} = 2.912 \times 10^{-3}$, and at this point the direction associated with the positive normal stretching rate $\hat{\mathbf{n}}^* = (\hat{n}_1^*, \hat{n}_2^*, \hat{n}_3^*)^{\mathrm{T}}$ is evaluated, finding $\hat{n}_1^* = 6.986 \times 10^{-4}, \hat{n}_2^* = 8.323 \times 10^{-1}, \hat{n}_3^* = 5.543 \times 10^{-1}$. Considering two nearby initial conditions $\mathbf{x}_1(0) = \mathbf{x}^*$ and $\mathbf{x}_2 = \mathbf{x}^* + \varepsilon\hat{\mathbf{n}}^*$, where ε is a small parameter, it is possible to evaluate the evolution of a small initial perturbation oriented along the direction of local normal positive stretching rate. The normalized distance $\|\mathbf{x}_1(t) - \mathbf{x}_2(t)\|/\varepsilon$ vs t is depicted in Fig. A.3 for $\varepsilon = 10^{-3}$. As can be observed, for short/intermediate times, this distance grows as a function of time, indicating that the occurrence of a positive local stretching rate is a manifestation of a local, albeit not invariant, normal instability.

To complete the analysis, it is useful to perform another simple numerical experiment. Instead of performing the normal stretching analysis of Eq. (A.1), a direction normal to the vector field $\mathbf{f}(\mathbf{x})$ and to the stoichiometric manifold $x_E + x_{ES} = x_{E,0}$ is selected, say $\hat{\mathbf{n}}_1 = (0, 1/\sqrt{2}, 1/\sqrt{2})^{\mathrm{T}}$, and the normal stretching rate $\widehat{\omega}_{v,1}$ associated with this direction evaluated. Subsequently, a second normal direction $\hat{\mathbf{n}}_2$ can be uniquely defined (modulo ± 1, which is immaterial in the estimate of stretching rates), which is tangent to $\mathscr{W}_2$ and normal to both $\mathbf{f}(\mathbf{x})$ and $\hat{\mathbf{n}}_2$. In this way $\widehat{\omega}_{v,2}(\mathbf{x})$ can be estimated, and $\widehat{\omega}_{v,2}(\mathbf{x})$ represents the maximum stretching rate normal to $\mathbf{f}(\mathbf{x})$, and lying in the tangent space to $\mathscr{W}_2$ at $\mathbf{x}$.

The behavior of $\widehat{\omega}_{v,1}$ and $\widehat{\omega}_{v,2}$ is depicted in Fig. A.2 (dashed lines). In this case, $\widehat{\omega}_{v,1}$ is identically vanishing. This stems from the observation that a stoichiometric manifold is defined by a linear equation

$$\mathbf{b} \cdot \mathbf{x} - C = \sum_{h=1}^{n} b_h x_h - C = 0 \tag{A.3}$$

where C is a constant and $\mathbf{b} = (b_1, \ldots, b_n)$ a vector possessing constant entries. If the dynamical system is n-dimensional, the stoichiometric manifold is a $(n-1)$-dimensional hyperplane. Along system orbits, from Eq. (A.3) follows $\mathbf{b} \cdot \mathbf{f}(\mathbf{x}) = 0$. By differentiating the latter equation with respect to $\mathbf{x}$, one obtains

$$\mathbf{b} \cdot \mathbf{J}(\mathbf{x}) = 0 \tag{A.4}$$

The constant vector $\mathbf{b}$, defining the stoichiometric manifold can be viewed as a vector normal to this linear manifold. Consequently, Eq. (A.4) implies that the normal stretching rate which is normal to the stoichiometric linear manifold is identically vanishing. This result can be straightforwardly extended to $(n-m)$-dimensional stoichiometric manifolds, expressed by a system of m linear constraints, $\mathbf{b}_h \cdot \mathbf{x} - C_h = 0, h = 1, \ldots, m$.

On the contrary, the second normal stretching rate $\widehat{\omega}_{v,2}$ is uniformly negative. Since $\hat{\mathbf{n}}^* \in T\mathscr{W}_2|_{\mathbf{x}^*}$, the stretching rate $\widehat{\omega}_{v,2}$ corresponds to the normal stretching rate associated with the two-dimensional dynamical

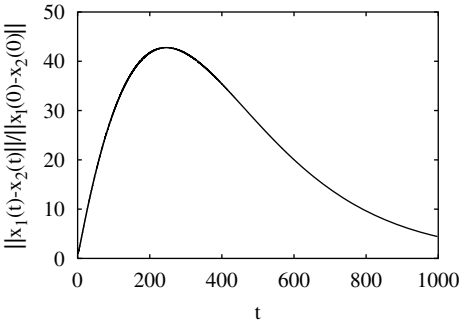

Fig. A.3. $\|\mathbf{x}_1(t) - \mathbf{x}_2(t)\|/\|\mathbf{x}_1(0) - \mathbf{x}_2(0)\|$ for two nearby trajectories of the Michaelis–Menten system, the initial distance of which is $\|\mathbf{x}_1(0) - \mathbf{x}_2(0)\| = \varepsilon = 10^{-3}$ along the normal direction possessing positive stretching rate.

system obtained from Eq. (A.1) when the stoichiometric constraint is explicitly accounted for, and the system dynamics is expressed exclusively as a function of x_S and x_{ES} (or equivalently of x_E).

To sum up, stretching rate analysis applied to chemical reacting systems displaying conservation laws, reproduces correctly the properties of the lower-dimensional slow manifold, which in the case of the Michaelis–Menten system behaves as a two-dimensional structure $\mathscr{W}_2$. The occurrence of positive stretching rates is due to the fact that stretching rate analysis explores and finds the direction of maximum normal stretching in the tangent subspace, which in principle may not satisfy the conservation law represented by stoichiometric constraints.

References

[1] U. Maas, R.W. Dibble, J. Warnatz, E. Zwicker, Combustion: Physical and Chemical Fundamentals, Modeling and Simulation, Experiments, Pollutant Formation, Springer-Verlag, Berlin, 1999.
[2] G.N. Stephanopulos, Metabolic Engineering: Principles and Applications, Academic Press, New York, 1998.
[3] U. Maas, S.B. Pope, Simplifying chemical kinetics: intrinsic low-dimensional manifolds in composition space, Combust. Flame 88 (1992) 239–264.
[4] U. Maas, S.B. Pope, Implementation of simplified chemical kinetics based on intrinsic low-dimensional manifolds, Proc. Combust. Inst. 24 (1992) 103–112.
[5] S. Singh, Y. Rastigejev, S. Paolucci, J.M. Powers, Viscous detonation in H_2–O_2–Ar using intrinsic low-dimensional manifolds and wavelet adaptive multilevel representation, Combust. Theory Modell. 5 (2002) 163–184.
[6] S.H. Lam, Using CSP to understand complex chemical kinetics, Combust. Sci. Technol. 89 (1993) 375–404.
[7] S.H. Lam, D.A. Goussis, The CSP method for simplifying kinetics, Int. J. Chem. Kinet. 26 (1994) 461–486.
[8] A.N. Gorban, I.V. Karlin, Method of invariant manifold for chemical kinetics, Chem. Eng. Sci. 58 (2003) 4751–4768.
[9] A.N. Gorban, I.V. Karlin, A. Yu. Zinovyev, Invariant grids for reaction kinetics, Physica A (2006), preprint.
[10] M.R. Roussel, S.J. Fraser, Geometry of the steady-state approximation: perturbation and accelerated convergence method, J. Chem. Phys. 93 (1990) 1072–1081.
[11] M.R. Roussel, S.J. Fraser, On the geometry of transient relaxation, J. Chem. Phys. 94 (1991) 7106–7113.
[12] A.N. Gorban, I.V. Karlin, A.Yu. Zinovyev, Constructive methods of invariant manifolds for kinetic problems, Phys. Rep. 396 (2004) 197–403.
[13] D. Lebiedz, Computing minimal entropy production trajectories: an approach to model reduction in chemical kinetics, J. Chem. Phys. 120 (2004) 6890–6897.
[14] A. Adrover, F. Creta, M. Giona, M. Valorani, V. Vitacolonna, Natural tangent dynamics with recurrent biorthogonaliations: a geometric computational approach to dynamical systems exhibiting slow manifolds and periodic/chaotic limit sets, Physica D 213 (2006) 121–146.
[15] C.W. Gear, T.J. Kaper, I.G. Kevrekidis, A. Zagaris, projecting to slow manifold: singularly perturbed systems and legacy codes, SIAM J. Appl. Dyn. Syst. 4 (2005) 711–732.
[16] D.A. Goussis, M. Valorani, An efficient iterative algorithm for the approximation of the fast and slow dynamics of stiff systems, J. Comp. Phys. 214 (2006) 316–346.
[17] A. Zagaris, H.G. Kaper, T.J. Kaper, Analysis of the computational singular perturbation reduction method for chemical kinetics, J. Nonlinear Sci. 14 (2004) 59–91.
[18] A. Zagaris, H.G. Kaper, T.J. Kaper, Two perspectives on reduction of ordinary differential equations, Math. Nachr. 278 (2005) 1629–1642.
[19] M.J. Davis, Low-dimensional manifolds in reaction–diffusion equations 1, J. Phys. Chem. A 110 (2006) 5235–5256.
[20] M. Hadjinicolaou, D.A. Goussis, Asymptotic solution of Stiff PDE's—the reaction diffusion equation, SIAM J. Sci. Comput. 20 (1999) 781–810.
[21] S. Singh, J.M. Powers, S. Paolucci, On slow manifolds of chemically reactive systems, J. Chem. Phys. 117 (2002) 1482–1496.
[22] D.A. Goussis, M. Valorani, F. Creta, H.N. Najm, Reactive and reactive–diffusive time scales in stiff reaction–diffusion systems, Prog. Comput. Fluid Dyn. 5 (2005) 316–326.
[23] R. Temam, Infinite-dimensional dynamical systems in mechanics and physics, Springer-Verlag, Berlin, 1997.
[24] J.C. Robinson, Infinite-Dimensional Dynamical Systems, Cambridge University Press, Cambridge, 2001.
[25] J.C. Robinson, Arbitrarily accurate approximate inertial manifolds of fixed dimension, Phys. Lett. A 230 (1997) 301–304.
[26] C. Foias, M.S. Jolly, I.G. Kevrekidis, G.R. Sell, E.S. Titi, On the computation of inertial manifolds, Phys. Lett. A 131 (1988) 433–436.
[27] M.S. Jolly, I.G. Kevrekidis, E.S. Titi, Approximate inertial manifolds for the Kuramoto–Sivashinsky equation: analysis and computations, Physica D 44 (1990) 38–60.
[28] A. Adrover, G. Continillo, S. Crescitelli, M. Giona, L. Russo, Wavelet-like collocation method for finite-dimensional reduction of distributed systems, Comput. Chem. Eng. 24 (2000) 2687–2703.
[29] S.-K. Tin, N. Kopell, N.C.K.R.T. Jones, Invariant manifolds and singularly perturbed boundary value problems, SIAM J. Numer. Anal. 31 (1984) 1558–1576.
[30] C. Jones, Geometric Singular Perturbation Theory, in: L. Arnold et al. (Eds.), Dynamical Systems, Springer-Verlag, Berlin, 1995, pp. 44–118.

[31] N. Fenichel, Geometric singular perturbation theory for ordinary differential equation, J. Differential Equations 31 (1979) 53–98.
[32] Z. Ren, S.B. Pope, Species reconstruction using pre-image curves, Proc. Comnust. Inst. 30 (2005) 1293–1300.
[33] E.N. Lorenz, V. Krishnamurthy, On the nonexistence of a slow manifold, J. Atmos. Sci. 44 (1987) 2940–2950.
[34] S.J. Jacobs, Existence of a slow manifold in a model system of equations, J. Atmos. Sci. 48 (1991) 893–901.
[35] E.N. Lorenz, The slow manifold—what is it? J. Atmos. Sci. 49 (1992) 2449–2451.
[36] F. Creta, A. Adrover, S. Cerbelli, M. Valorani, M. Giona, Slow manifold structure in explosive kinetics I—bifurcations of points-at-infinity in prototypical models, J. Phys. Chem. A 110 (2006) 13464–13474.
[37] H.G. Kaper, T.J. Kaper, Asymptotic analysis of two reduction methods for systems of chemical reactions, Physica D 165 (2002) 66–93.
[38] I. Goldfarb, V. Goldshtein, U. Maas, Comparative analysis of two asymptotic approaches based on integral manifolds, IMA J. Appl. Math. 69 (2004) 353–374.
[39] M.W. Hirsch, C.C. Pugh, M. Shub, Invariant manifolds, Lecture Notes in Mathematics, vol. 583, Springer-Verlag, Berlin, 1977.
[40] A. Massias, D. Diamantis, E. Mastorakos, D.A. Goussis, An algorithm for the construction of global reduced mechanisms with CSO data, Combust. Flame 117 (1999) 685–708.
[41] S.K. Scott, Chemical Chaos, Clarendon Press, Oxford, 1991.
[42] A. Goldbeter, Biochemical Oscillations and Cellular Rhythms, Cambridge University Press, Cambridge, 1996.
[43] K.D. Mease, S. Bharadway, S. Iravanchy, Timescale analysis for nonlinear dynamical systems, J. Guidance Control Dyn. 26 (2003) 318–330.
[44] R. T Skodje, M.J. Davis, geometric simplification of complex kinetic systems, J. Phys. Chem. A 105 (2001) 10356–10365.
[45] H.D.I. Abarbanel, R. Brown, J.J. Sidorowich, L.Sh. Tsimring, The analysis of observed chaotic data in physical systems, Rev. Mod. Phys. 65 (1993) 1331–1392.
[46] F. Verhulst, Invariant manifolds in dissipative dynamical systems, Acta Appl. Math. 87 (2005) 229–244.
[47] V. Bykov, I. Goldfarb, V. Gol'dsthein, U. Maas, On a modified version of ILDM approach: asymptotic analysis based on integral manifolds, IMA J. Appl. Math. 71 (2006) 359–382.
[48] L.B. Ryashko, E.E. Shnol, On exponentially attracting invariant manifolds of ODEs, Nonlinearity 16 (2003) 147–160.
[49] N.N. Semenov, Zur theorie des verbrennungprozesses, Z. Phys. 48 (1928) 571–581.
[50] A. Varma, M. Morbidelli, H. Wu, Parametric Sensitivity in Chemical Systems, Cambridge University Press, Cambridge, 1999.
[51] M.J. Davis, R.T. Skodije, Geometric investigation of low-dimensional manifolds in systems approaching equilibrium, J. Chem. Phys. 111 (1999) 859–874.
[52] L. Perko, Differential Equations and Dynamical Systems, 2nd ed., Springer-Verlag, New York, 1996.
[53] E.N. Lorenz, Deterministic nonperiodic flow, J. Atmos. Sci. 20 (1963) 130–141.
[54] J. Guckenheimer, P. Holmes, Nonlinear Oscillations, Dynamical Systems, and Bifurcations of Vector Fields, Springer-Verlag, New York, 1993.
[55] A. Katok, B. Hasselblatt, Introduction to the Modern Theory of Dynamical Systems, Encyclopaedia of Mathematics and its Applications, vol. 54, Cambridge University Press, Cambridge, 1995.
[56] K.D. Mease, U. Topcu, Two-timescale nonlinear dynamics and slow manifold determination, in: Proc. AIAA Guidance and Control Conference, San Francisco 2005, pp. 307–315.
[57] A. Adrover, S. Cerbelli, M. Giona, Exterior algebra-based algorithms to estimate Liapunov spectra and stretching statistics in high-dimensional and distributed systems, Int. J. Bifurcat. Chaos 12 (2002) 353–368.
[58] J. Elezgaray, A. Arneodo, Crisis-induced intermittent bursting in reaction–diffusion chemical systems, Phys. Rev. Lett. 68 (1992) 714–717.
[59] A. Adrover, G. Continillo, S. Crescitelli, M. Giona, L. Russo, Construction of approximate inertial manifold by decimation of collocation equations of distributed parameter systems, Comput. Chem. Eng. 26 (2002) 113–123.
[60] M.D. Graham, I.G. Kevrekidis, Alternative approaches to the Karhunen–Loeve decomposition for modal reduction and data analysis, Comput. Chem. Eng. 20 (1996) 495–506.
[61] F. Takens, Detecting Strange Attractors in Turbulence, Lecture Notes in Mathematics, 898, Springer-Verlag, Berlin, 1981, pp. 366–382.
[62] F.A. Williams, Combustion Theory, Benjamin Cummings, Menlo Park, 1985.
[63] B.J. Matkowsky, G.I. Sivashinsky, Propagation of a pulsating reaction front in solid fuel combustion, SIAM J. Appl. Math. 35 (1978) 465–478.
[64] G.I. Sivashinsky, Nonlinear analysis of hydrodynamic instability in laminar flames. Part I Derivation of basic equations, Acta Astronaut. 4 (1977) 1177–1206.
[65] A. Bayliss, B.J. Matkowsky, From traveling waves to chaos in combustion, SIAM J. Appl. Math. 50 (1990) 437–459.
[66] O. Roussel, K. Schneider, A. Tsigulin, H. Bockhorn, A conservative fully adaptive multiresolution algorithm for parabolic PDEs, J. Comp. Phys. 188 (2003) 493–523.
[67] O. Roussel, K. Schneider, Adaptive numerical simulation for pulsating planar flames for large Lewis and Zeldovich ranges, Comm. Nonlinear Sci. Numer. Simulat. 11 (2006) 463–480.
[68] V. Giovangigli, M. Massot, Entropic structure of multicomponent reactive flows with partial equilibrium reduced chemistry, Math. Meth. Appl. Sci. 27 (2004) 739–768.